

Parallel, Asymptotically Optimal Algorithms for Moving Target Traveling Salesman Problems

Anoop Bhat¹, Geordan Gutow², Bhaskar Vundurthy¹,
Zhongqiang Ren³, Sivakumar Rathinam⁴, and Howie Choset¹

Abstract—The Moving Target Traveling Salesman Problem (MT-TSP) seeks an agent trajectory that intercepts several moving targets, within a particular time window for each target. In the presence of generic nonlinear target trajectories or kinematic constraints on the agent, no prior algorithm guarantees convergence to an optimal MT-TSP solution. Therefore, we introduce the Iterated Random Generalized (IRG) TSP framework. The key idea behind IRG is to alternate between randomly sampling a set of agent configuration-time points, corresponding to interceptions of targets, and finding a sequence of interception points by solving a generalized TSP (GTSP). This alternation enables asymptotic convergence to the optimum. We introduce two parallel algorithms within the IRG framework. The first algorithm, IRG-PGLNS, solves GTSPs using PGLNS, our parallelized extension of the state-of-the-art solver GLNS. The second algorithm, Parallel Communicating GTSPs (PCG), solves GTSPs corresponding to several sets of points simultaneously. We present numerical results for three variants of the MT-TSP: one where intercepting a target only requires coming within a particular distance, another where the agent is a variable-speed Dubins car, and a third where the agent is a redundant robot arm. We show that IRG-PGLNS and PCG both converge faster than a baseline based on prior work.

Index Terms—Motion planning, traveling salesman problem, combinatorial search, parallelization, Dubins car.

I. INTRODUCTION

The Traveling Salesman Problem (TSP) is a classic optimization problem with broad applications in various fields, including logistics, manufacturing, and robotics [1], [2]. Given a set of targets (often called “locations” or “cities”) and the cost of travel between each target pair, the TSP seeks a minimum-cost order of targets for an agent to visit. However, several robotic applications require planning to visit moving targets: midair refueling [3], optimization of fishing routes [4], [5], resupplying ships at sea [6], surveillance [7]–[9], and intercepting dangerous projectiles [10]–[12]. These applications lead to the Moving Target TSP (MT-TSP) [12], which is more challenging than the TSP, as it seeks to simultaneously optimize not only the visiting order of targets, but also a kinematically feasible agent trajectory that arrives at each

¹Robotics Institute at Carnegie Mellon University, 5000 Forbes Ave., Pittsburgh, PA 15213, USA. Emails: {agbhat, ggutow, pvundurt, choset}@andrew.cmu.edu

²Mechanical and Aerospace Engineering at Michigan Technological University, Houghton, MI 49931. Email: gmgutow@mtu.edu

³Global College at Shanghai Jiao Tong University, Shanghai, China. Email: zhongqiang.ren@sjtu.edu.cn

⁴Department of Mechanical Engineering and Department of Computer Science and Engineering at Texas A&M University, College Station, TX 77843. Email: srathinam@tamu.edu

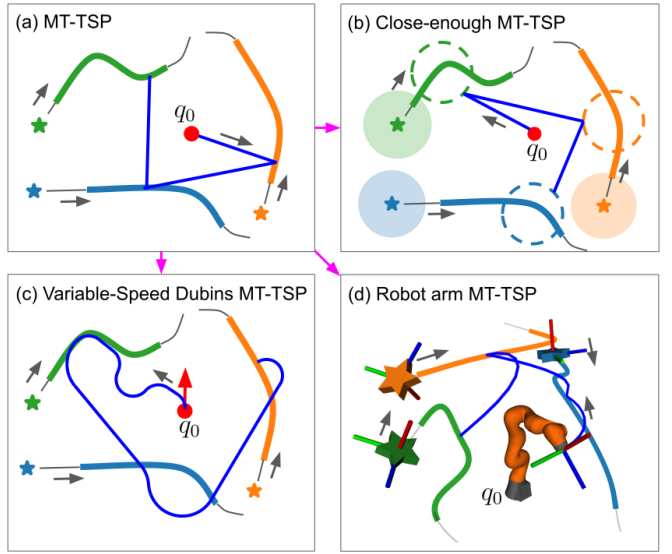


Fig. 1. MT-TSP and three variants. In all subfigures, targets (stars) move along trajectories with time windows shown in bold colored lines. Targets’ locations are shown at $t = 0$. Agent’s trajectory (blue) begins at initial configuration q_0 and intercepts all targets. In this work, we consider Hamiltonian paths, where the agent does not need to return to q_0 . (a) MT-TSP, where the agent is limited by a maximum speed. (b) Close-enough MT-TSP, where agent has a maximum speed, and each target is surrounded by a disc of positions where it may be intercepted. Filled discs are centered at the targets’ positions at $t = 0$, and dashed, unfilled discs indicate disc locations at moment of interception. (c) Variable-speed Dubins MT-TSP, where agent has a minimum speed, maximum speed, and a minimum turning radius that increases with speed. (d) Robot arm MT-TSP. Agent is a 7-DOF arm (Kuka iiwa), where each joint has a speed limit. Intercepting a target requires matching the end-effector pose with the target’s pose. Poses are visualized at $t = 0$ with reference frames.

target within a specified time window. Moreover, unlike in the TSP, the travel costs between targets are not fixed in the MT-TSP, but rather depend on the location in space and time at which the agent intercepts each target.

In this paper, we address the MT-TSP, as well as three generalizations, shown in Fig. 1:

- **Close-enough MT-TSP:** the agent needs only to pass through a disc centered on the moving target. This is motivated by scenarios such as wireless data transmission, where the disc represents the communication range.
- **Variable-Speed Dubins MT-TSP:** the agent has a minimum and maximum speed, as well as a minimum turning radius that increases with its speed. This is motivated by applications with ground vehicles and fixed-wing UAVs.
- **Robot Arm MT-TSP:** the agent is a redundant robotic arm that must intercept moving targets (e.g. parts on a conveyor belt) using its end effector.

All of the above variants of the MT-TSP generalize the TSP

and are thus NP-hard [12], [13]. Furthermore, due to the presence of time windows, even finding a feasible solution for these MT-TSP variants is NP-complete [14]. To our knowledge, no prior work addresses any of the three MT-TSP variants above in the presence of time windows and nonlinear target trajectories. The closest related work is [15], which addresses the close-enough MT-TSP without time windows for a Dubins car. In this paper, we address all three variants in the presence of time windows using a single algorithmic framework.

We call our framework Iterated Random Generalized (IRG) TSP. Algorithms within the IRG framework operate within one or more parallel processes. Each process performs several iterations, where each iteration constructs a *sample point graph* containing a finite number of space-time points sampled along each target's trajectory. The sample point graph is divided into clusters, where the points corresponding to a particular target form a cluster. An edge connects a point s from one cluster to a point s' in a different cluster if a transition from s to s' is kinematically feasible. For a robot whose only kinematic constraint is a speed limit, kinematically feasible simply means that there is enough time to travel from s to s' .

After constructing a sample point graph, we solve a Generalized Traveling Salesman Problem (GTSP), which seeks a minimum-cost tour that visits exactly one point from each cluster. In subsequent iterations, each process generates a new set of sample points that includes both randomly sampled points and points selected from all processes' previous GTSP solutions. We prove that our approach converges asymptotically to an optimal solution through this iterative refinement.

Algorithms in the IRG framework differ in the number of parallel processes and the method of solving the underlying GTSP. Our first presented IRG algorithm, called IRG-PGLNS, uses one process, but uses a parallel GTSP solver, which we call Parallel Generalized Large Neighborhood Search (PGLNS). PGLNS extends the state-of-the-art GTSP solver Generalized Large Neighborhood Search (GLNS) [16] using ideas from parallel large neighborhood search [17]. Our second presented IRG algorithm, called Parallel Communicating GTSPs (PCG), runs several parallel processes, where each process uses GLNS to solve its GTSP.

Note that the sample point graphs in the MT-TSP are incomplete graphs, as it is often kinematically infeasible to travel between pairs of sampled points. Our analysis shows that state-of-the-art GTSP solvers, such as GLNS [16], struggle to find feasible solutions on these incomplete graphs. To overcome this challenge, we present a new approach to finding a feasible GTSP solution, adapting pruning methods from the literature on TSP with time windows [18]. This is critically important for the IRG framework to find its first feasible solution, upon which it then iterates.

We validate our methods with extensive numerical experiments, demonstrating improved convergence speeds of IRG-PGLNS and PCG over a baseline based on the memetic algorithm from [15]. In addition, we demonstrate the importance of different components of the algorithms via ablation studies. We also show that PCG outperforms IRG-PGLNS for the close-enough MT-TSP, and that IRG-PGLNS outperforms

PCG for the variable-speed Dubins MT-TSP. Finally, we show that our initial solution generation method, common to all IRG variations, finds feasible solutions faster than existing GTSP solution methods.

II. RELATED WORK

A. MT-TSP

Existing optimal algorithms for the MT-TSP, based on mixed-integer programming (MIP), are limited to linear or piecewise-linear trajectories of targets and assume that the agent can move omnidirectionally [10], [19]–[21], while our work does not make these assumptions. [22] lower bounds the optimal cost when the trajectories of the targets are generic, and the objective is to minimize the agent's travel time. For finding feasible agent trajectories in the presence of generic target trajectories and motion constraints on the agent, sub-optimal algorithms exist [8]–[10], [15], [22]–[26]. Sampling-based algorithms [10], [22], [24], [25] proceed by sampling the trajectories of targets into points in space-time, then finding a sequence of points to visit by solving a GTSP. Our work combines these prior sampling-based methods for the MT-TSP with sampling-based methods for the close-enough TSP, Dubins TSP, and TSPs for robot arms, as described in the rest of this section. We additionally incorporate resampling to achieve asymptotic optimality, as well as parallelization for speed. Another suboptimal method for the MT-TSP is the memetic algorithm presented in [15], which addresses a Dubins close-enough MT-TSP without time windows. In our experiments, we adapt the method from [15] to handle time windows and use it as a baseline. Finally, [27] provides a suboptimal method for a close-enough MT-TSP without time windows using large neighborhood search, but is specialized to linear target trajectories.

B. Close-Enough TSP with Static Targets

The close-enough TSP [28] seeks the shortest path in space that visits a set of static targets, where visiting a target requires entering a disc centered at the target's location. Optimal algorithms have been developed for the close-enough TSP [29], [30]. The computational burden of optimal methods has motivated the development of suboptimal methods [31]–[34]. Our work on the close-enough MT-TSP extends the method from [31], [32], which samples each target's disc into points in space, then solves a GTSP to find an order of targets to visit and a sampled point for each target. Other suboptimal approaches for the close-enough TSP include the variable neighborhood search in [33] and the genetic algorithm in [34].

C. Dubins TSP with Static Targets

The Dubins TSP [35] seeks the shortest path in space that visits a set of stationary target positions such that the path satisfies a minimum turning radius constraint. The challenge in the Dubins TSP that distinguishes it from the classic TSP is determining the agent's heading angle at each target's position: if the heading angle at each target is given, then the cost of travel between each pair of targets is given by the length

of a Dubins path [36], and the problem reduces to a classic TSP. While there are no optimal solvers for the Dubins TSP, methods have been developed to lower bound the optimal cost [37]. A common suboptimal approach is to sample a set of headings for each target, then solve a GTSP to select an order of targets to visit as well as the sampled heading angle at each target [38]–[41]. Our work combines this approach with sampling-based methods for the MT-TSP. Another suboptimal approach for the Dubins TSP is the decoupled approach in [42], which determines a sequence of targets using a Euclidean TSP and then optimizes the heading angles along the sequence. Alternatively, the approach in [43] combines an evolutionary algorithm with machine learning.

Prior work [44] has also considered a variable-speed Dubins TSP where the agent’s minimum turning radius is not fixed, but is instead a function of its speed, and there is an upper limit on the derivative of the speed. To simplify the problem, [44] restricts the agent to move at a constant speed when turning and only accelerate when moving straight. Additionally, [44] only allows the agent to select from a finite set of speeds during constant-speed segments. Our work does not consider limits on the derivative of the speed, but considers moving targets, in contrast to [44]. Similarly to [44], we only allow the agent to select from a finite set of speeds.

D. Robot Arm TSP with Static Targets

Variants of the TSP for a robot arm generally seek a minimum-cost path or trajectory through a robot arm’s configuration space such that the end-effector pose passes through a given set of stationary target poses [45]. Different variants arise depending on whether the arm is redundant, as well as the constraints the arm must satisfy, e.g. joint speed limits [46], joint torque limits [47], and/or obstacle avoidance [48]–[51]. Our work considers a redundant arm with joint speed limits and no obstacles. One of the challenges in solving a TSP for a redundant arm is that along with finding an ordering of target end-effector poses, we must also select from the infinite number of arm configurations that can achieve each target pose. Our approach to handling redundancy in the robot arm MT-TSP extends [49], which samples a finite set of arm configurations at each end-effector pose, then solves a GTSP to select a sequence of configurations to visit. Another approach for handling redundancy for TSPs with robot arms is the decoupled approach from RoboTSP [50], which finds a sequence of targets first by solving a TSP in end-effector space, then optimizes the arm configuration at each target with a sampling-based method, given the sequence. Additionally, [51] applies a genetic algorithm to optimize the sequence of targets and arm configurations simultaneously.

E. Parallel TSP Algorithms

Parallel algorithms exist for the TSP [17], [52]–[56], but they only provide means of optimizing an ordering of targets, whereas in the MT-TSP, we must also optimize the time and configuration at which the agent intercepts each target. Optimal MT-TSP algorithms [10], [19]–[21] using MIP solvers such as Gurobi [57] can leverage the parallel capabilities

of the MIP solver, but these optimal algorithms carry the limitations discussed in Section II-A. Sampling-based MT-TSP algorithms using integer programming (IP) to solve their GTSP can similarly leverage their IP solver’s parallel capabilities, but IP’s computation time scales poorly with the number of targets, which we demonstrate in our experiments in Section VII. Currently GLNS [16], the most scalable method of solving GTSPs, is serial, and one of our contributions is the combination of parallel large neighborhood search [17] with GLNS [16] in the new parallel GTSP solver PGLNS.

III. PROBLEM SETUP

A. Problem Statement

We consider an agent with configuration space \mathcal{Q}_a , which is determined by the particular MT-TSP variant that is being considered. The agent has an initial configuration $q_{a,0}$, which may correspond to a point robot that must get “close enough” to a target, a Dubins car, or a robotic arm. Let the agent’s trajectory be $\tau_a : \mathbb{R}^+ \rightarrow \mathcal{Q}_a$. We assume that in each agent configuration q_a , there is a set \mathcal{A}_{q_a} of admissible agent velocities, and we say that a trajectory τ_a is *kinematically feasible* in an interval $[t_0, t_f]$ if $\dot{\tau}_a(t) \in \mathcal{A}_{\tau_a(t)}$ for all $t \in [t_0, t_f]$. We use \mathcal{A}_{q_a} to incorporate kinematic constraints, such as a minimum turning radius or a speed limit.

We denote the set of moving targets as $\mathcal{I} = \{1, 2, \dots, n_{\text{tar}}\}$, where n_{tar} is the number of targets. Each target moves through a space \mathcal{Q}_{tar} , which we define for each MT-TSP variant in Section III-B. Note that \mathcal{Q}_{tar} is the configuration space of an individual target, so the joint configuration space of all the targets would be $\mathcal{Q}_{\text{tar}}^{n_{\text{tar}}}$. The trajectory of target i is $\tau_i : \mathbb{R}^+ \rightarrow \mathcal{Q}_{\text{tar}}$. The time interval where target i must be intercepted, i.e. the *time window* of target i , is $[\underline{t}_i, \bar{t}_i] \subset \mathbb{R}^+$, where \underline{t}_i is the start time and \bar{t}_i is the end time. We assume that we are given an *interception function* $\Xi_i : \mathcal{Q}_a \times \mathcal{Q}_{\text{tar}} \rightarrow \{0, 1\}$, where if $\Xi_i(q_a, q_{\text{tar},i}) = 1$, the agent configuration q_a is said to *intercept* the target configuration $q_{\text{tar},i}$. If there exists $t_i \in [\underline{t}_i, \bar{t}_i]$ such that $\Xi_i(\tau_a(t_i), \tau_i(t_i)) = 1$, we say that the agent trajectory τ_a intercepts target i . In the close-enough MT-TSP and robot arm MT-TSP, the cost function is the distance traveled in \mathcal{Q}_a . In the variable-speed Dubins MT-TSP, the cost function is the agent’s distance traveled in \mathbb{R}^2 .

Problem: The MT-TSP seeks a minimum-cost, kinematically feasible trajectory τ_a that starts at $q_{a,0}$ at $t = 0$ and intercepts all targets.

B. Preliminaries

IRG is a generic framework designed for problems that fit the description above. To apply IRG to a specific MT-TSP variant, we must specify \mathcal{Q}_a , \mathcal{Q}_{tar} , \mathcal{A}_{q_a} , and Ξ_i as well as the following functions:

- $\text{RandConfig}_i : [\underline{t}_i, \bar{t}_i] \rightarrow \mathcal{Q}_a$, which generates a random $q_a \in \mathcal{Q}_a$ that intercepts target i at a given $t \in [\underline{t}_i, \bar{t}_i]$.
- $\text{TrajExists} : \mathcal{Q}_a \times \mathbb{R}^+ \times \mathcal{Q}_a \times \mathbb{R}^+ \rightarrow \{0, 1\}$, where $\text{TrajExists}(q_a, t, q_a', t') = 1$ if a kinematically feasible agent trajectory τ_a exists with $\tau_a(t) = q_a$ and $\tau_a(t') = q_a'$, and $\text{TrajExists}(q_a, t, q_a', t') = 0$ otherwise,

- $\text{GetTraj} : \mathcal{Q}_a \times \mathbb{R}^+ \times \mathcal{Q}_a \times \mathbb{R}^+ \rightarrow (\mathbb{R}^+)^{\mathcal{Q}_a}$, where $(\mathbb{R}^+)^{\mathcal{Q}_a}$ is the set of functions mapping from \mathbb{R}^+ to \mathcal{Q}_a , i.e. the set of agent trajectories. $\text{GetTraj}(q_a, t, q_a', t')$ attempts to return a kinematically feasible agent trajectory τ_a with $\tau_a(t) = q_a$ and $\tau_a(t') = q_a'$ and returns NULL if no trajectory is found.

Next, we specify these sets and functions for the close-enough, variable-speed Dubins, and robot arm MT-TSPs.

1) *Close-Enough MT-TSP*: In the close-enough MT-TSP, $\mathcal{Q}_a = \mathcal{Q}_{\text{tar}} = \mathbb{R}^2$. The agent has a maximum speed v_{\max} . The set of admissible velocities at any configuration q_a is $\mathcal{A}_{q_a} = \{q_a : \|\dot{q}_a\| \leq v_{\max}\}$. Each target i is associated with a radius r_i , and $\Xi_i(q_a, q_{\text{tar},i}) = 1$ if and only if $\|q_a - q_{\text{tar},i}\| \leq r_i$. $\text{RandConfig}_i(t)$ samples $\theta \in \mathbb{S}^1$ uniformly at random, then returns $\tau_i(t) + r_i \begin{bmatrix} \cos \theta \\ \sin \theta \end{bmatrix}$, i.e. it randomly samples from the boundary of target i 's disc¹.

$\text{TrajExists}(q_a, t, q_a', t')$ checks if $\|q_a - q_a'\| \leq v_{\max}(t' - t)$. $\text{GetTraj}(q_a, t, q_a', t')$ returns a constant-velocity trajectory from (q_a, t) to (q_a', t') , defined by $\tau(t'') = q_a + (q_a' - q_a) \frac{t'' - t}{t' - t}$.

2) *Variable-Speed Dubins MT-TSP*: In the variable-speed Dubins MT-TSP, $\mathcal{Q}_a = SE(2)$ and $\mathcal{Q}_{\text{tar}} = \mathbb{R}^2$. The agent, a variable-speed Dubins car [58], has a minimum speed² v_{\min} , a maximum speed v_{\max} , and a maximum turning rate ω_{\max} . While for a standard Dubins car, the minimum turning radius is fixed, a variable-speed Dubins car's minimum turning radius increases with its speed, i.e. for a speed v , the minimum turning radius is $\frac{v}{\omega_{\max}}$. Consider an agent configuration $q_a = (p, \phi)$ with $p \in \mathbb{R}^2$ and $\phi \in \mathbb{S}^1$. The velocity of the agent is $(\dot{p}, \dot{\phi})$. The set of admissible velocities at q_a is

$$\mathcal{A}_{q_a} = \{(\dot{p}, \dot{\phi}) : \dot{p} = \|\dot{p}\| \begin{bmatrix} \cos \phi \\ \sin \phi \end{bmatrix} \text{ and } |\dot{\phi}| \in [0, \omega_{\max}] \text{ and } \|\dot{p}\| \in [v_{\min}, v_{\max}]\}. \quad (1)$$

Consider a target configuration $q_{\text{tar},i} \in \mathcal{Q}_{\text{tar}}$. $\Xi_i(q, q_{\text{tar},i}) = 1$ if and only if $p = q_{\text{tar},i}$. $\text{RandConfig}_i(t)$ samples a heading angle $\phi \in \mathbb{S}^1$ uniformly at random, then returns $q_a = (\tau_i(t), \phi)$.

To define TrajExists , we assume that the agent can only select from a finite set of speeds $\mathcal{S}_{\text{speed}} = \{v_1, v_2, \dots, v_{n_{\text{speed}}}\}$, where n_{speed} is the number of allowed speeds. We additionally assume that between two consecutive interceptions of targets, the agent does not change its speed. $\text{TrajExists}(q_a, t, q_a', t')$ returns 1 if and only if for some $v \in \mathcal{S}_{\text{speed}}$, a path in $SE(2)$ exists beginning at q_a and terminating at q_a' with length $v(t' - t)$ and curvature no larger than $\frac{\omega_{\max}}{v}$ (equivalently, turning radius no smaller than $\frac{v}{\omega_{\max}}$). We check path existence using the methods from [59].

$\text{GetTraj}(q_a, t, q_a', t')$ proceeds in two steps. The first step generates a curvature-bounded path with length $v(t' - t)$ beginning at q_a and terminating at q_a' , for the smallest $v \in \mathcal{S}_{\text{speed}}$ for which such a path exists. The second step returns the agent

¹By only sampling on the disc boundaries, we sacrifice asymptotic optimality in degenerate problem instances where all optimal agent trajectories stay inside the disc of some target for the entirety of its time window.

²When we refer to speed, curvature, or length of a trajectory or path for a variable-speed Dubins car, we refer to the position component of its trajectory or path, not the combination of the position and orientation components.

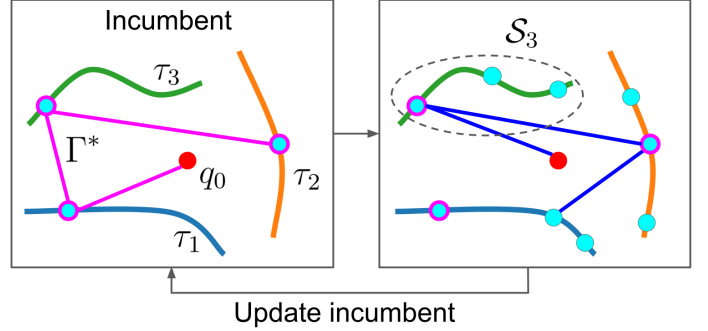


Fig. 2. An iteration of tour improvement in IRG-PGLNS. The trajectory corresponding to the incumbent tour (the least-cost tour found so far) is shown in pink. Points in the incumbent tour are outlined in pink. To improve the incumbent tour, as seen in the right-hand box, we generate a set of sample points for each target, including several random points and the point from the incumbent. For example, S_3 is the set of points for target 3. We then solve a GTSP to find an updated incumbent.

trajectory that follows this path with fixed speed v . We again use the methods from [59] when generating the path.

3) *Robot Arm MT-TSP*: In the robot arm MT-TSP, $\mathcal{Q}_a = [\underline{q}^1, \bar{q}^1] \times [\underline{q}^2, \bar{q}^2] \times \dots \times [\underline{q}^{\dim \mathcal{Q}_a}, \bar{q}^{\dim \mathcal{Q}_a}]$, where $[\underline{q}^j, \bar{q}^j]$ is the interval of allowable angles for joint j , and $\dim \mathcal{Q}_a$ is the number of joints in the arm. Additionally, $\mathcal{Q}_{\text{tar}} = SE(3)$. Each joint j has a speed limit v_{\max}^j . The set of admissible velocities at any configuration q_a is $\mathcal{A}_{q_a} = \{q_a : |\dot{q}_a^j| \leq v_{\max}^j \forall j\}$, where q_a^j is the j th element of q_a . Let $FK : \mathcal{Q}_a \rightarrow SE(3)$ be the forward kinematic map. For $q_a \in \mathcal{Q}_a$ and $q_{\text{tar},i} \in \mathcal{Q}_{\text{tar}}$, $\Xi_i(q_a, q_{\text{tar},i}) = 1$ if and only if $FK(q_a) = q_{\text{tar},i}$.

$\text{RandConfig}_i(t)$ generates an inverse kinematics (IK) solution for the end-effector pose $\tau_i(t)$. When there are multiple IK solutions, we have several options for redundancy resolution. For many 7 DOF arms [60]–[62], a unique IK solution is specified when we specify a *global configuration parameter* h_{gc} from some finite set \mathcal{H}_{gc} and a self-motion parameter h_{sm} from some $\mathcal{H}_{\text{sm}} \subseteq \mathbb{R}^{\dim \mathcal{Q}_a - 6}$; thus, $\text{RandConfig}_i(t)$ samples some $(h_{\text{gc}}, h_{\text{sm}})$ uniformly at random from $\mathcal{H}_{\text{gc}} \times \mathcal{H}_{\text{sm}}$, then computes the unique IK solution specified by $\tau_i(t)$, h_{gc} , and h_{sm} . Alternatively, we can use numerical IK, where we randomly sample an initial guess in \mathcal{Q}_a for a numerical IK solver. If the IK solution q_a does not fall within joint angle limits, RandConfig_i returns NULL.

$\text{TrajExists}(q_a, t, q_a', t')$ is implemented by checking if $|q_a^j - q_a'^j| \leq v_{\max}^j(t' - t)$ for all $j \in \{1, 2, \dots, \dim \mathcal{Q}_a\}$. $\text{GetTraj}(q_a, t, q_a', t')$ returns a constant-velocity trajectory from (q_a, t) to (q_a', t') , defined by $\tau(t'') = q_a + (q_a' - q_a) \frac{t'' - t}{t' - t}$.

IV. IRG-PGLNS ALGORITHM

In this section, we present our first instantiation of the IRG framework, which we call IRG-PGLNS, due to its use of our novel GTSP solver, PGLNS. IRG-PGLNS is described by Alg. 1 and illustrated in Fig. 2. IRG-PGLNS searches the space of *tours*, where a tour is a sequence of points (configuration-time pairs) in $\mathcal{Q}_a \times \mathbb{R}^+$ beginning with $(q_{a,0}, 0)$, such that each target is intercepted by one point in the sequence. Upon termination, IRG-PGLNS uses GetTraj to connect each pair of consecutive points in its best tour Γ^* to form a trajectory³. We search the space of tours because in

³In this work, we do not require continuity of the trajectory's velocity.

the variable-speed Dubins MT-TSP, checking if a trajectory exists between two points (i.e. invoking `TrajExists`) is computationally cheaper than computing the trajectory using `GetTraj`. We leverage the ability to compute a tour's cost without computing the associated trajectory.

Throughout IRG-PGLNS, we refer to the best tour we have found so far as the *incumbent*, denoted as Γ^* . IRG-PGLNS initializes Γ^* (Alg. 1, Line 1) using the `GenerateInitialTour` procedure, detailed in Section IV-A. IRG-PGLNS then begins its tour improvement loop (Line 2). Each iteration of this loop generates a set of sample points \mathcal{S}_i for each target i . \mathcal{S}_i contains the point where Γ^* visits target i , denoted by `GetInterceptionPoint`(i, Γ^*), as well as n_{rand} points randomly sampled using Alg. 3. Alg. 3 repeatedly samples a time t in target i 's time window at random, then samples an agent configuration q_a using `RandConfig` $_i$, to obtain a random point (q_a, t) .

After constructing \mathcal{S}_i for all targets, IRG-PGLNS finds a new incumbent Γ^* via `TourViaGTSP`, described in Section IV-B. We pass the current Γ^* as a seed tour that `TourViaGTSP` improves upon. When planning time runs out, IRG-PGLNS returns the trajectory associated with Γ^* .

Algorithm 1: IRG-PGLNS

```

1  $\Gamma^* = \text{GenerateInitialTour}();$ 
2 while Time limit has not been reached do
3   for  $i \in \{1, 2, \dots, n_{\text{tar}}\}$  do
4      $\mathcal{S}_i = \{\text{GetInterceptionPoint}(i, \Gamma^*)\} \cup$ 
5        $\text{RandomSamples}(i, n_{\text{rand}});$ 
6    $\Gamma^* = \text{TourViaGTSP}(\{\mathcal{S}_i\}_{i \in \mathcal{I}}, \Gamma^*);$ 
7 Return trajectory associated with  $\Gamma^*;$ 

```

A. Initial Tour Generation

`GenerateInitialTour`, described by Alg. 2, begins by randomly sampling a set of points \mathcal{S}_i for each target i (Lines 3-4). Alg. 2 then seeks a tour Γ^* intercepting each target i at a point in \mathcal{S}_i via `TourViaGTSP` (Section IV-B). In contrast to Alg. 1, we do not pass a seed tour to `TourViaGTSP`, since we do not have a seed tour to pass. For a given set of sample points, `TourViaGTSP` may not find a feasible tour. If `TourViaGTSP` finds a feasible tour Γ^* , Alg. 2 returns Γ^* (Lines 6-7). Otherwise, if there is time left, Alg. 2 adds more samples to each \mathcal{S}_i and attempts to find a tour again.

B. Finding Tour via GTSP

The `TourViaGTSP` function, used in Alg. 1 and Alg. 2, seeks a tour where the point intercepting target i is an element of \mathcal{S}_i . We first construct a *sample point graph* $\mathcal{G} = (\mathcal{V}, \mathcal{E})$, where \mathcal{V} is the set of nodes and \mathcal{E} is the set of edges. \mathcal{V} contains all sample points and the pairing of $q_{a,0}$ with time 0, i.e. $\mathcal{V} = \bigcup_{i \in \mathcal{I}} \mathcal{S}_i \cup \{(q_{a,0}, 0)\}$. An edge connects node (q_a, t) to node (q'_a, t') if `TrajExists`($(q_a, t, q'_a, t') = 1$ and the nodes belong to different sets \mathcal{S}_i . The edge cost depends on the particular problem variant. In the close-enough and robot

Algorithm 2: `GenerateInitialTour`

```

1  $\mathcal{S}_i = \emptyset$  for all  $i \in \mathcal{I};$ 
2 while Time limit has not been reached do
3   for  $i \in \{1, 2, \dots, n_{\text{tar}}\}$  do
4      $\mathcal{S}_i = \mathcal{S}_i \cup \text{RandomSamples}(i, n_{\text{rand, init}});$ 
5    $\Gamma^* = \text{TourViaGTSP}(\{\mathcal{S}_i\}_{i \in \mathcal{I}});$ 
6   if  $\Gamma^*$  is not NULL then
7     return  $\Gamma^*;$ 
8 return NULL;

```

Algorithm 3: `RandomSamples` (i, n)

```

1  $\mathcal{S} = \emptyset;$ 
2 for  $k \in \{1, 2, \dots, n\}$  do
3    $q_a = \text{NULL};$ 
4   while  $q_a$  is NULL do
5      $t = \text{UniformRandomSample}([t_i, \bar{t}_i]);$ 
6      $q_a = \text{RandConfig}_i(t);$ 
7    $\mathcal{S} = \mathcal{S} \cup \{(q_a, t)\};$ 
8 return  $\mathcal{S};$ 

```

arm MT-TSPs, the edge cost is $\|q_a' - q_a\|$. In the variable-speed Dubins MT-TSP, the edge cost is $v^*(q_a, t, q_a', t')(t' - t)$, where $v^*(q_a, t, q_a', t')$ is the minimum $v \in \mathcal{S}_{\text{speed}}$ such that the path existence check performed by `TrajExists` succeeds (the path existence check is described in Section III-B2). We can find a tour by finding a sequence of nodes in \mathcal{G} beginning at $(q_{a,0}, 0)$ and containing one node in each \mathcal{S}_i . This is the same as solving a GTSP on \mathcal{G} .

IRG-PGLNS solves the GTSP using one of two methods. If no seed tour is passed, we use the depth-first search (DFS) described in Section IV-C. If a seed tour is passed, IRG-PGLNS solves the GTSP using PGLNS, which is described in Section IV-D. We only run PGLNS if we have a seed tour because we have found that on incomplete graphs such as \mathcal{G} , PGLNS, as well as its predecessor GLNS, struggle to find a feasible tour unless we provide one, which is shown in the experiments (Section VII-I).

PGLNS, like its predecessor GLNS, requires that a matrix of integer edge costs be passed to the solver, where the entry for row i , column j is the cost of edge (i, j) . Note that \mathcal{G} is an incomplete graph, i.e. there are some edges (i, j) that do not exist in \mathcal{G} . We call such nonexistent edges *infeasible* edges, as opposed to *feasible* edges that actually exist in \mathcal{G} . To interface with PGLNS, we still need to populate costs for infeasible edges. To populate the cost matrix, we first multiply all feasible edge costs by 100, round to the nearest integer, and populate the corresponding entries in the cost matrix, effectively rounding all edge costs to two decimal places. For all infeasible edges, we need the cost to be large enough that any tour traversing an infeasible edge will have larger cost than the incumbent; thus, we set the cost equal to the cost of the current incumbent, computed using scaled and rounded edge costs, plus one.

To guarantee asymptotic optimality despite using a sub-optimal GTSP solver such as PGLNS, `TourViaGTSP` does not immediately return the tour found by the GTSP solver. Instead, after obtaining a tour Γ^{tmp} from the GTSP solver, we also generate a random tour Γ^{rand} using the current sets \mathcal{S}_i . If Γ^{rand} has lower cost than Γ^{tmp} , `TourViaGTSP` returns Γ^{rand} ; otherwise, `TourViaGTSP` returns Γ^{tmp} . This additional step of generating Γ^{rand} is only of theoretical value, as Γ^{rand} is almost never chosen over Γ^{tmp} in practice.

C. Solving GTSP via Depth-First Search

When generating the initial tour, we solve the GTSP in Section IV-B using the DFS in Alg. 4, aiming to quickly find a feasible solution without considering its cost. Before beginning the main loop, we construct a set $\text{BEFORE}[s]$ for each node $s \in \mathcal{V}$ (Lines 1-3), containing all targets that have no sample points reachable from s , i.e. all targets that must be visited before s . The construction of BEFORE is inspired by [18], which addresses the TSP with time windows.

After constructing BEFORE , we initialize a stack of *search nodes* (Line 4), where a search node is a tuple $u = (\mathcal{U}, s)$, with $\mathcal{U} \subseteq \mathcal{I}$ and $s \in \mathcal{V}$. A search node represents the set of tours through \mathcal{G} visiting the same set of targets \mathcal{U} (perhaps in different orders) and terminating with the same sample point $s \in \mathcal{V}$. We maintain a backpointer for each search node u , denoted as $u.\text{bp}$, equal to a search node previously popped from the stack. Once we set a backpointer for a search node, the search node represents a particular tour, which we can reconstruct by traversing the backpointer chain. We also use a CLOSED set (Line 5) to avoid re-expanding search nodes.

Each iteration of the main search loop pops a search node $u = (\mathcal{U}, s)$ from the stack, and if $\mathcal{U} = \mathcal{I}$, the search terminates and returns a tour reconstructed from u (Lines 7-11). If $\mathcal{U} \neq \mathcal{I}$, we generate the *successor G-nodes* of u (Line 12), which are the nodes $s' \in \mathcal{V}$ satisfying the following conditions:

- 1) $(s, s') \in \mathcal{E}$.
- 2) $s' \notin \mathcal{S}_i$ for any $i \in \mathcal{U}$.
- 3) $\text{BEFORE}[s'] \subseteq \mathcal{U}$.

Condition 1 ensures that the tour represented by $(\mathcal{U} \cup \{s'\}, s')$ is a feasible tour in \mathcal{G} . Condition 2 ensures that each target is visited once. This guarantees that the maximum depth of the DFS is fixed, and thus the DFS terminates, which is used in the probabilistic completeness proof in Section VI. Condition 3 ensures that by visiting s' , we do not prevent any unvisited targets from being visited.

Finally, for each successor \mathcal{G} -node s' , we generate a successor search node $u' = (\mathcal{U} \cup \{s'\}, s')$, then push u' onto the stack (Lines 13-16). We push successors onto the stack in order of decreasing edge cost from s to s' , such that the least-cost successor gets popped from the stack next. The search nodes and successor relationships in Alg. 4 implicitly form a directed acyclic graph (DAG), so we refer to Alg. 4 as DAG-DFS in the experiments.

D. PGLNS

When a seed tour Γ^* is passed to `TourViaGTSP`, IRG-PGLNS solves the GTSP using a parallel extension of GLNS

Algorithm 4: DepthFirstSearch

```

1 BEFORE = dict();
2 for  $s \in \mathcal{V}$  do
3   BEFORE[s] =
4      $\{i \in \mathcal{I} : s \notin \mathcal{S}_i \text{ and } (\forall s' \in \mathcal{S}_i)((s, s') \notin \mathcal{E})\}$ ;
5 STACK =  $[(\emptyset, (q_{a,0}, 0))]$ ;
6 CLOSED =  $\emptyset$ ;
7 while STACK is not empty do
8    $u = (\mathcal{U}, s) = \text{STACK.pop}()$ ;
9   if  $u \in \text{CLOSED}$  then continue;
10  CLOSED.insert( $u$ );
11  if  $\mathcal{U} = \mathcal{I}$  then
12    return ReconstructTour ( $u$ );
13  for  $s'$  in  $u.\text{successorGNodes}()$  do
14     $u' = (\mathcal{U} \cup \{s'\}, s')$ ;
15    if  $u' \in \text{CLOSED}$  then continue;
16     $u'.\text{bp} = u$ ;
17    STACK.push( $u'$ );
17 return NULL;

```

[16] which we call PGLNS. PGLNS is described by Alg. 5. Like GLNS, PGLNS runs n_{warm} “warm” trials. Each warm trial begins by initializing a current tour Γ^c , a counter i_{term} , a scalar temperature θ , a cooling rate r_{cool} , and several locks (Lines 2 to 6). The determination of the temperature and cooling rate using the warm trial counter is explained in Section 5.3 of [16]. The warm trial then runs several threads, each of which runs an inner loop (Line 8).

Each iteration of a thread j ’s inner loop copies $\Gamma^{c,j}$, removes several nodes from $\Gamma^{c,j}$, then inserts nodes back into $\Gamma^{c,j}$ (Lines 12-14). The nodes to remove are selected using a removal heuristic h^r , and the nodes to insert are selected using an insertion heuristic h^i . The heuristics are randomly sampled from the same bank of heuristics used in [16]. If the modified $\Gamma^{c,j}$ is accepted (determined using the simulated annealing criteria from [16]), thread j updates Γ^c to $\Gamma^{c,j}$ (Lines 15-18). Then, if $\Gamma^{c,j}$ has lower cost than Γ^* thread j updates Γ^* (Lines 19-22). Thread j then performs the local optimizations described in [16] on $\Gamma^{c,j}$, and if it is still better than Γ^* (i.e. if another thread did not find a better tour), thread j updates Γ^* again (Lines 27-30).

Every time we update Γ^* , we reset i_{term} (Line 25), and if we do not update Γ^* in the current iteration, we increment i_{term} (Line 35). A thread terminates its inner loop when i_{term} reaches a threshold (Lines 9-11), which is set to a smaller number if Γ^* has never been improved in the current warm trial, and a larger number thereafter, as in [16]. The n_{term} parameter corresponds to the `num_iterations` parameter in GLNS, and the thresholds $n_{\text{term}}/6$ and $n_{\text{term}}/4$ correspond to GLNS’s fast mode.

V. PCG

We now present our second instantiation of the IRG framework, which we call PCG. PCG shares many of the subroutines of IRG-PGLNS, but employs a different form of parallelization. Instead of using the parallel solver PGLNS to solve

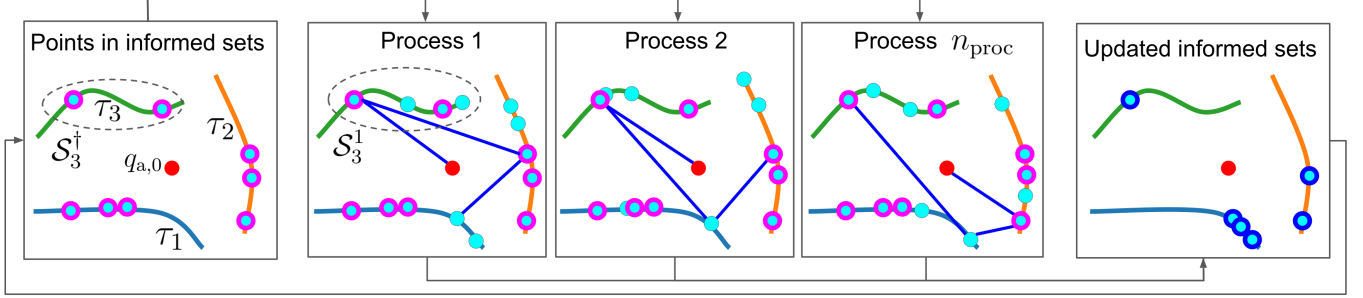


Fig. 3. Illustration of an iteration of trajectory improvement in PCG. The main process maintains an informed set of points \mathcal{S}_i^\dagger for each target i . Points in the current iteration's informed sets are outlined in pink. Each child process $j \in \{1, 2, \dots, n_{\text{proc}}\}$ generates a set of sample points \mathcal{S}_i^j for each target i , containing the points from the current \mathcal{S}_i^\dagger , as well as random points unique to process j . Each child process then solves a GTSP, finding a sequence of points beginning at $q_{a,0}$ visiting one point per target. The main process then updates the informed set for each target i to contain all visited points associated with target i from all child processes.

GTSPs, PCG uses the serial solver GLNS, but solves several GTSPs simultaneously, each corresponding to a different set of sample points. PCG is described by Alg. 6, which we refer to as the main process. We also provide an illustration in Fig. 3. PCG begins by finding an initial tour Γ^* using the same method as Alg. 1. After finding Γ^* , PCG initializes an *informed set* \mathcal{S}_i^\dagger for each target. In particular, it initializes \mathcal{S}_i^\dagger as a singleton set, containing the point $(q_a, t) \in \mathcal{Q}_a \times \mathbb{R}^+$ at which Γ^* visits target i (Line 4).

After initializing the informed sets, PCG begins its tour improvement loop (Line 5). Each iteration of this loop runs n_{proc} parallel child processes. Each child process j generates a set of sample points \mathcal{S}_i^j for each target i (Lines 7-8). \mathcal{S}_i^j contains all points in \mathcal{S}_i^\dagger , as well as n_{rand} randomly sampled points unique to process j . After constructing \mathcal{S}_i^j , each process j finds a tour Γ^j by solving a GTSP (Line 8). Rather than using PGLNS at this step, we use the serial GLNS. We found that if we set n_{proc} equal to the number of cores on our computer and also tried to parallelize GLNS, then PCG's performance degraded due to running more total threads than the number of cores. While there is potential for combining PCG with PGLNS, e.g. using 2 PCG processes with 5 PGLNS threads per process on a 10-core computer, we leave this combination to future work.

After finding a tour Γ^j , each process j generates a list of points P^j , which we call process j 's *informed list* (Lines 10-12). The i th element $P^j[i]$ is the point at which Γ^j visits target i . We then update the informed sets, such that \mathcal{S}_i^\dagger contains all points associated with target i from all informed lists in the current iteration (Lines 13-14). Finally, we update Γ^* to the best tour found by any child process (Line 15). If there is time left, PCG runs its child processes again using the new informed sets. Otherwise, PCG returns the trajectory associated with Γ^* (Line 16).

In PCG, a child process cannot begin a new iteration of the loop on Line 5 until all other processes have finished their previous loop iteration. We additionally experimented with an asynchronous version of PCG, where as soon as a child process finishes invoking `TourViaGTSP`, it retrieves the latest informed lists from the other processes (even if some of the lists have not been updated), constructs its own informed set, and begins the next iteration of the loop on Line 5. We found that this did not provide noticeable benefits and pursued

the synchronous algorithm.

VI. THEORETICAL ANALYSIS

In this section, we show that under appropriate assumptions, all algorithms in the IRG framework are probabilistically complete: that is, if a feasible MT-TSP trajectory exists, the probability of finding a feasible trajectory approaches 1 as runtime tends to infinity. We additionally prove the asymptotic optimality of the IRG framework: that is, as runtime tends to infinity, the returned trajectory's cost converges to the optimum with probability 1. We specifically prove probabilistic completeness and asymptotic optimality for IRG-PGLNS, and PCG straightforwardly inherits these properties.

Assumption 1. For any $q_a, t, q_a', t' \in \mathcal{Q}_a \times \mathbb{R}^+ \times \mathcal{Q}_a \times \mathbb{R}^+$, if `TrajExists` (q_a, t, q_a', t') , then `GetTraj` (q_a, t, q_a', t') returns a kinematically feasible agent trajectory τ_a with $\tau_a(t) = q_a$ and $\tau_a(t') = q_a'$.

Assumption 1 trivially holds for the close-enough MT-TSP and robot arm MT-TSP, since `GetTraj` simply returns a straight-line trajectory from (q_a, t) to (q_a', t') . For the variable-speed Dubins MT-TSP, while [59] provides a necessary and sufficient condition for the existence of a trajectory from (q_a, t) to (q_a', t') for a given speed v , it does not offer a constructive method for generating such a trajectory when one exists. Nevertheless, in our experiments, we successfully used numerical methods to compute a feasible trajectory for every tour returned by each algorithm in Section VII.

Let \mathcal{F} be the set of feasible trajectories for an MT-TSP instance. For the variable-speed Dubins MT-TSP, we also require \mathcal{F} to satisfy the assumptions in Section III-B2, i.e. each $\tau_a \in \mathcal{F}$ maintains constant speed between consecutive interceptions of two targets and only travels at speeds in $\mathcal{S}_{\text{speed}}$.

Let $\mathcal{L}_{\mathcal{Q}_a} = \prod_{i=1}^{n_{\text{tar}}} \mathcal{Q}_a \times [t_i, \bar{t}_i]$, i.e. the set of lists of (configuration, time) pairs, with one pair per target. For a list $l_{\mathcal{Q}_a} \in \mathcal{L}_{\mathcal{Q}_a}$, if there exists a trajectory $\tau_a \in \mathcal{F}$ intercepting each target i at $l_{\mathcal{Q}_a}[i]$, we say $l_{\mathcal{Q}_a}$ is *achieved* by τ_a .

Next, note that for each MT-TSP variant we consider, $\text{RandConfig}_i(t)$ samples a parameter from some underlying sample space, then maps this parameter to an agent configuration q_a . For example, as described in Section III, in the close-enough and variable-speed Dubins variants, the underlying

Algorithm 5: PGLNS (Γ^*)

```

1 for  $i_{\text{warm}} = 1, 2, \dots, n_{\text{warm}}$  do
2    $\Gamma^c = \text{Copy}(\Gamma^*)$ ;
3    $i_{\text{term}} = 1$ ;
4   improved = false;
5    $\theta, r_{\text{cool}} = \text{SetTempAndCoolingRate}(i_{\text{warm}})$ ;
6   Initialize locks  $l^c, l^*, l^{i_{\text{term}}}, l^\theta$ ;
7   parallel for  $j = 1, 2, \dots, n_{\text{thread}}$  do
8     while true do
9       With Lock ( $l^{i_{\text{term}}}$ )
10      if (not improved and  $i_{\text{term}} > n_{\text{term}}/6$ ) or
11        (improved and  $i_{\text{term}} > n_{\text{term}}/4$ ) or other
12        thread broke then
13          break
14
15        $h^r, h^i = \text{RandomlySelectHeuristics}()$ ;
16       With Lock( $l^c$ ),  $\Gamma^{c,j} = \text{Copy}(\Gamma^c)$ ;
17        $\Gamma^{c,j} = \text{RemoveAndInsert}(\Gamma^{c,j}, h^r, h^i)$ ;
18       With Lock( $l^\theta$ ),  $\theta^j = \text{Copy}(\theta)$ ;
19       With Lock( $l^c$ ) accept = Accept ( $\Gamma^{c,j}, \Gamma^c, \theta^j$ );
20       if accept then
21         With Lock( $l^c$ ),  $\Gamma^c = \Gamma^{c,j}$ ;
22         With Lock( $l^*$ )
23           update_best =
24             Cost( $\Gamma^{c,j}$ ) < Cost( $\Gamma^*$ );
25           if update_best then
26              $\Gamma^* = \text{Copy}(\Gamma^{c,j})$ ;
27
28         if update_best then
29           With Lock( $l^{i_{\text{term}}}$ )
30              $i_{\text{term}} = 1$ ;
31             improved = true;
32           Locally reoptimize  $\Gamma^{c,j}$ 
33           With Lock( $l^*$ )
34             if Cost( $\Gamma^{c,j}$ ) < Cost( $\Gamma^*$ ) then
35                $\Gamma^* = \text{Copy}(\Gamma^{c,j})$ ;
36
37           With Lock( $l^c$ )
38             if Cost( $\Gamma^{c,j}$ ) < Cost( $\Gamma^c$ ) then
39                $\Gamma^c = \text{Copy}(\Gamma^{c,j})$ ;
40
41         else
42           With Lock( $l^{i_{\text{term}}}$ )  $i_{\text{term}} = i_{\text{term}} + 1$ ;
43
44       With Lock( $l^\theta$ )  $\theta = \theta r_{\text{cool}}$ 
45
46 return  $\Gamma^*$ ;

```

Algorithm 6: PCG

```

1  $\Gamma^* = \text{GenerateInitialTour}()$ ;
2 if  $\Gamma^*$  is NULL then return NULL;
3 for  $i \in \mathcal{I}$  do
4    $\mathcal{S}_i^\dagger = \{\text{GetInterceptionPoint}(i, \Gamma^*)\}$ ;
5   // Tour improvement
6   while Time limit has not been reached do
7     parallel for  $j \in \{1, 2, \dots, n_{\text{proc}}\}$  do
8       for  $i \in \{1, 2, \dots, n_{\text{tar}}\}$  do
9          $\mathcal{S}_i^j = \mathcal{S}_i^\dagger \cup \text{RandomSamples}(i, n_{\text{rand}})$ ;
10         $\Gamma^j = \text{TourViaGTSP}(\{\mathcal{S}_i^j\}_{i \in \mathcal{I}}, \Gamma^*)$ ;
11        Initialize  $P^j$  as list of length  $n_{\text{tar}}$ ;
12        for  $i \in \{1, 2, \dots, n_{\text{tar}}\}$  do
13           $P^j[i] = \text{GetInterceptionPoint}(i, \Gamma^j)$ ;
14
15       for  $i \in \mathcal{I}$  do
16          $\mathcal{S}_i^\dagger = \{P^1[i], P^2[i], \dots, P^{n_{\text{proc}}}[i]\}$ ;
17
18       Set  $\Gamma^*$  equal to  $\Gamma^j$  with least cost;
19
20 return trajectory associated with  $\Gamma^*$ ;

```

space is \mathbb{S}^1 , and in the robot arm variant, the underlying space is $\mathcal{H}_{\text{gc}} \times \mathcal{H}_{\text{sm}}$ for analytical IK and \mathcal{Q}_a for numerical IK. In general, let \mathcal{H} be the underlying sample space for the variant at hand, and let $\text{MapSample}_i : \mathcal{H} \times [t_i, \bar{t}_i] \rightarrow \mathcal{Q}_a$ be the function used by RandConfig_i to map a sample in \mathcal{H} and a time in $[t_i, \bar{t}_i]$ to an agent configuration in \mathcal{Q}_a . MapSample_i is defined as follows for the three variants.

- Close-enough MT-TSP: $\text{MapSample}_i(h_i, t) = \tau_i(t) + r_i \begin{bmatrix} \cos(h_i) \\ \sin(h_i) \end{bmatrix}$.
- Variable-speed Dubins MT-TSP: $\text{MapSample}_i(h_i, t) = (\tau_i(t), h_i)$.
- Robot arm MT-TSP: $\text{MapSample}_i(h_i, t)$ invokes the appropriate IK solver.

Let $\mathcal{L}_{\mathcal{H}} = \prod_{i=1}^{n_{\text{tar}}} (\mathcal{H} \times [t_i, \bar{t}_i])$. Define a function $\text{MapList} : \mathcal{L}_{\mathcal{H}} \rightarrow \mathcal{L}_{\mathcal{Q}_a}$ which maps a list $l_{\mathcal{H}}$ defined by $l_{\mathcal{H}}[i] = (h_i, t_i)$ to a list $l_{\mathcal{Q}_a}$ with $l_{\mathcal{Q}_a}[i] = (\text{MapSample}_i(h_i, t_i), t_i)$. For $l_{\mathcal{H}} \in \mathcal{L}_{\mathcal{H}}$, if $\text{MapList}(l_{\mathcal{H}})$ is achieved by some $\tau_a \in \mathcal{F}$, we say $l_{\mathcal{H}}$ is achieved by τ_a as well.

$\mathcal{L}_{\mathcal{H}}$ is a product of several sets, which we call components. Each component may have finite or infinite cardinality⁴. We define each component as a metric space by endowing each finite component with the discrete metric and each infinite component with the Euclidean metric [63]. We endow $\mathcal{L}_{\mathcal{H}}$ with the metric defined by summing the metrics of its components. We use this metric when defining Lipschitz continuity of functions with domain $\mathcal{L}_{\mathcal{H}}$. We endow all other spaces with the Euclidean metric when necessary. We also endow each metric space with its metric topology, defining an open subset as a union of open balls under the space's metric [63]. For any metric space \mathcal{X} and $p, p' \in \mathcal{X}$, let $d(p, p')$ be the distance

⁴Finite cardinality specifically occurs in the robot arm MT-TSP when using analytical IK, since $\mathcal{H} = \mathcal{H}_{\text{gc}} \times \mathcal{H}_{\text{sm}}$, and \mathcal{H}_{gc} is finite.

from p to p' under the metric. For any $p \in \mathcal{X}$ and $\mathcal{S} \subseteq \mathcal{X}$, let $d(p, \mathcal{S}) = \inf_{p' \in \mathcal{S}} d(p, p')$.

Theorem 1. (Probabilistic Completeness) Suppose there exists a non-empty open set $\mathcal{N} \subseteq \mathcal{L}_{\mathcal{H}}$ such that each $l_{\mathcal{H}} \in \mathcal{N}$ is achieved by some $\tau_a \in \mathcal{F}$. Given Assumption 1, as the number of iterations of Alg. 2 tends to infinity, the probability that Alg. 2, and therefore IRG-PGLNS, produces a feasible MT-TSP trajectory approaches 1.

Proof. At the k th iteration of the loop in Alg. 2 Line 2, let $(^k h_i, ^k t_i)$ be the final random sample drawn for target i , and define $^k l_{\mathcal{H}} \in \mathcal{L}_{\mathcal{H}}$ by $^k l_{\mathcal{H}}[i] = (^k h_i, ^k t_i)$. We sampled each $(^k h_i, ^k t_i)$ uniformly from $\mathcal{H} \times [t_i, \bar{t}_i]$, so $^k l_{\mathcal{H}}$ is sampled from a uniform distribution over $\mathcal{L}_{\mathcal{H}}$, which places positive measure on nonempty open subsets, including \mathcal{N} . Thus as k approaches infinity, the probability that $^k l_{\mathcal{H}} \in \mathcal{N}$ approaches 1. Once we have $^k l_{\mathcal{H}} \in \mathcal{N}$, the tour obtained by computing $^k l_{\mathcal{Q}_a} = \text{MapList}(^k l_{\mathcal{H}})$, then sorting $^k l_{\mathcal{Q}_a}$ in order of increasing time values and prepending $(q_{a,0}, 0)$, will be feasible for the GTSP. Alg. 4 will return this tour or some other feasible tour, ensuring that Alg. 1 produces a feasible tour Γ^* . Assumption 1 then guarantees that we connect the consecutive points in Γ^* to return a feasible trajectory. \square

We now begin the asymptotic optimality proofs. First, we define the *corresponding* target sequence of $l_{\mathcal{H}} \in \mathcal{L}_{\mathcal{H}}$ as the sequence obtained by sorting the interception times in $l_{\mathcal{H}}$. For a set \mathcal{S} in a topological space, let $\overline{\mathcal{S}}$ be the closure of \mathcal{S} .

Lemma 1. Let $\mathcal{N} \subseteq \mathcal{L}_{\mathcal{H}}$ be open and nonempty. Then there is a nonempty open set $\mathcal{N}' \subseteq \mathcal{N}$ such that all lists in $\overline{\mathcal{N}'}$ have the same corresponding target sequence.

Proof. Let $l_{\mathcal{H}}^{\#}$ be any list in \mathcal{N} . In the rest of this proof, for each $i \in \mathcal{I}$, let $t_i^{\#}$ be the interception time for target i in $l_{\mathcal{H}}^{\#}$. We now apply a series of perturbations to $l_{\mathcal{H}}^{\#}$ such that all targets have distinct interception times. In particular, while there is any pair of targets i, j with $t_i^{\#} = t_j^{\#}$, we perform the following steps. (1) Choose an open, nonempty ball $\mathcal{B} \subseteq \mathcal{N}$ centered at $l_{\mathcal{H}}^{\#}$ (one must exist by definition of the metric topology [63]), and let r be the radius of \mathcal{B} . (2) Let i and j be two targets with $t_i^{\#} = t_j^{\#}$. (3) Let $a = \min_{k \in \mathcal{I}, t_i^{\#} \neq t_k^{\#}} |t_i^{\#} - t_k^{\#}|$. (4) Perform the perturbation $t_i^{\#} \leftarrow t_i^{\#} + \min\{r/2, a/2\}$. Now $t_i^{\#}$ is distinct from all other interception times in $l_{\mathcal{H}}^{\#}$, and $l_{\mathcal{H}}^{\#}$ is still in \mathcal{B} and thus in \mathcal{N} .

Let $\delta = \min_{i,j \in \mathcal{I}, i \neq j} |t_i^{\#} - t_j^{\#}|$. Since distinct targets have distinct interception times in $l_{\mathcal{H}}^{\#}$ after performing the sequence of perturbations above, $\delta > 0$. Suppose there is some $l_{\mathcal{H}} \in \mathcal{N}$ with a different corresponding sequence of targets than $l_{\mathcal{H}}^{\#}$, and for each target i , let t_i be its interception time in $l_{\mathcal{H}}$. Since $l_{\mathcal{H}}^{\#}$ and $l_{\mathcal{H}}$ have different corresponding target sequences, there must be some pair of targets i, j such that $t_i^{\#} < t_j^{\#}$ and $t_i > t_j$, i.e. $t_j^{\#} - t_i^{\#} > 0$ and $t_j - t_i < 0$. By the definition of δ , $\delta \leq t_j^{\#} - t_i^{\#}$. Adding the positive value $-(t_j - t_i)$ to the RHS, we have $\delta < t_j^{\#} - t_i^{\#} - (t_j - t_i) = (t_j^{\#} - t_j) + (t_i - t_i^{\#}) \leq |t_j^{\#} - t_j| + |t_i - t_i^{\#}| \leq \sqrt{2} \sqrt{(t_j^{\#} - t_j)^2 + (t_i - t_i^{\#})^2}$, where the last inequality follows from [64], proof of Corollary

3.2. This means $\frac{1}{\sqrt{2}}\delta < \sqrt{(t_j^{\#} - t_j)^2 + (t_i - t_i^{\#})^2}$. Therefore, $d(l_{\mathcal{H}}^{\#}, l_{\mathcal{H}}) > \frac{1}{\sqrt{2}}\delta$. Thus any $l_{\mathcal{H}}$ with a different corresponding target sequence than $l_{\mathcal{H}}^{\#}$ must be farther than $\frac{1}{\sqrt{2}}\delta$ from $l_{\mathcal{H}}^{\#}$. Let \mathcal{N}' be the open ball of radius $\frac{1}{\sqrt{2}}\delta$ centered at $l_{\mathcal{H}}^{\#}$. By the above argument, all $l_{\mathcal{H}} \in \overline{\mathcal{N}'}$ must have the same corresponding target sequence as $l_{\mathcal{H}}^{\#}$. Since $\delta > 0$, \mathcal{N}' is nonempty. \square

Lemma 2. Suppose the trajectories of the targets are Lipschitz on their time windows. For the close-enough MT-TSP and variable-speed Dubins MT-TSP, MapList is Lipschitz on $\mathcal{L}_{\mathcal{H}}$.

Now consider the robot arm MT-TSP, for the KUKA iiwa arm considered in this paper, and assume we are using analytical IK. For any $l_{\mathcal{H}}^{\#} \in \mathcal{L}_{\mathcal{H}}$ such that for all configurations in MapList($l_{\mathcal{H}}^{\#}$), (i) the shoulder-wrist vector (defined in [60]) has nonzero norm (ii) joint angles 1, 3, 5, and 7 do not equal π , and (iii) joint angles 2, 4, and 6 do not equal 0 or π , then there is an open $\mathcal{N}^{\#} \subseteq \mathcal{L}_{\mathcal{H}}$ containing $l_{\mathcal{H}}^{\#}$ such that MapList is Lipschitz on $\mathcal{N}^{\#}$.

Proof. Since MapList concatenates invocations of MapSample $_i$, showing that MapList is Lipschitz on $\mathcal{L}_{\mathcal{H}}$ requires showing that MapSample $_i$ is Lipschitz on the i th component of $\mathcal{L}_{\mathcal{H}}$, i.e. $\mathcal{H} \times [t_i, \bar{t}_i]$, for each $i \in \mathcal{I}$. For the close-enough MT-TSP, MapSample $_i$ is Lipschitz on $\mathcal{H} \times [t_i, \bar{t}_i]$, since MapSample $_i(\theta, t)$ only consists of cosine, sine, and addition operations, all of which are Lipschitz, as well as τ_i , which is Lipschitz by assumption. For the variable-speed Dubins MT-TSP, MapSample $_i$ is Lipschitz on $\mathcal{H} \times [t_i, \bar{t}_i]$, since MapSample $_i(\phi, t)$ concatenates $\tau_i(t)$ and ϕ , which is a linear operation, and τ_i is Lipschitz on $[t_i, \bar{t}_i]$ by assumption. Thus MapList is Lipschitz on $\mathcal{L}_{\mathcal{H}}$ for the close-enough MT-TSP and variable-speed Dubins MT-TSP.

Now consider the robot arm MT-TSP for the iiwa. We proceed by constructing an open set \mathcal{P}_i for each $i \in \mathcal{I}$ where MapSample $_i$ is Lipschitz on $\overline{\mathcal{P}_i}$, then letting $\mathcal{N}^{\#} = \prod_{i=1}^{n_{\text{tar}}} \mathcal{P}_i$.

Computing MapSample $_i(h_i, \tau_i(t_i))$ via analytical IK requires computing a shoulder-wrist vector $v_i = f_{\text{sw}}(\tau_i(t_i))$, then normalizing v_i (see [60]). Normalization is only Lipschitz on sets where every element's norm can be lower-bounded by the same constant $c > 0$. Let $(h_i^{\#}, t_i^{\#}) = l_{\mathcal{H}}^{\#}[i]$. Let $v_i^{\#} = f_{\text{sw}}(\tau_i(t_i^{\#}))$. Let $\overline{\mathcal{B}_i}$ be the closed ball centered at $(0, 0, 0)$ with radius $\|v_i^{\#}\|/2$. $\mathcal{C}_i = \mathbb{R}^3 \setminus \overline{\mathcal{B}_i}$ is open, and normalization is Lipschitz on $\overline{\mathcal{C}_i}$, since each element's norm is lower-bounded by $\|v_i^{\#}\|/2$, and $\|v_i^{\#}\|/2 > 0$ by assumption (i).

Additionally, f_{sw} is Lipschitz [60], and τ_i is Lipschitz by assumption, so $f_i : [t_i, \bar{t}_i] \rightarrow \mathbb{R}^3$, defined by $f_i(t_i) = f_{\text{sw}}(\tau_i(t_i))$, is Lipschitz, and thus continuous. Since f_i is continuous and \mathcal{C}_i is open, the preimage of \mathcal{C}_i under f_i , i.e. $f_i^{-1}(\mathcal{C}_i)$, is open. Since normalization is Lipschitz on $\overline{\mathcal{C}_i}$, and f_i is Lipschitz, $\hat{f}_i(t_i) = \frac{f_i(t_i)}{\|f_i(t_i)\|}$ is Lipschitz on $f_i^{-1}(\overline{\mathcal{C}_i})$. Since $f_i^{-1}(\mathcal{C}_i) \subseteq f_i^{-1}(\overline{\mathcal{C}_i})$, $\hat{f}_i(t_i)$ is Lipschitz on $f_i^{-1}(\mathcal{C}_i)$.

For each joint $j \in \{1, 3, 5, 7\}$, MapSample $_i(h_i, t_i)$ computes the j th joint angle q_i^j as $\text{arctan2}(g^j(\tau_i(t_i), h_i, \hat{f}_i(t_i)))$, where g^j is defined for each j in [60], returning a (y, x) pair. For joints

$j \in \{2, 4, 6\}$, $\text{MapSample}_i(h_i, t_i)$ computes g_i^j as $\arccos(g^j(\tau_i(t_i), h_i, \hat{f}_i(t_i)))$, where g^j is again defined for each j in [60], but scalar-valued. All the g^j functions are Lipschitz. For each j , let $g_i^{j\#} = g^j(\tau_i(t_i), h_i\#, \hat{f}_i(t_i\#))$.

For each $j \in \{1, 3, 5, 7\}$, $g_i^{j\#} \notin \{0\} \times (-\infty, 0]$ by assumption (ii), and $\{0\} \times (-\infty, 0]$ is closed, so $d(g_i^{j\#}, \{0\} \times (-\infty, 0])$ is some $\delta_i^j > 0$. Also, for each $j \in \{2, 4, 6\}$, $g_i^{j\#} \notin \{-1, 1\}$ by assumption (iii), and $\{-1, 1\}$ is closed, so $d(g_i^{j\#}, \{-1, 1\})$ is some $\delta_i^j > 0$. For each joint j , let \mathcal{B}_i^j be the open ball centered at $g_i^{j\#}$ with radius $\delta_i^j/2$. For joints $j \in \{1, 3, 5, 7\}$, arctan2 is Lipschitz on $\overline{\mathcal{B}_i^j}$, and for joints $j \in \{2, 4, 6\}$, \arccos is Lipschitz on $\overline{\mathcal{B}_i^j}$. Let $g_i : \mathcal{H} \times f_i^{-1}(\mathcal{C}_i) \rightarrow \mathbb{R}^{11}$ be defined by

$$g_i(h_i, t_i) = (g^1(\tau_i(t_i), h_i, \hat{f}_i(t_i)), g^2(\tau_i(t_i), h_i, \hat{f}_i(t_i)), \dots, g^7(\tau_i(t_i), h_i, \hat{f}_i(t_i))) \quad (2)$$

Since \hat{f}_i is Lipschitz on $\overline{f_i^{-1}(\mathcal{C}_i)}$, g_i is Lipschitz and thus continuous on $\mathcal{H} \times \overline{f_i^{-1}(\mathcal{C}_i)}$. Since g_i is continuous on $\mathcal{H} \times \overline{f_i^{-1}(\mathcal{C}_i)}$, and the sets \mathcal{B}_i^j are open, and $\mathcal{H} \times \overline{f_i^{-1}(\mathcal{C}_i)}$ is open, we have that $\mathcal{P}_i = g_i^{-1} \left(\prod_{j=1}^7 \mathcal{B}_i^j \right) \cap (\mathcal{H} \times \overline{f_i^{-1}(\mathcal{C}_i)})$ is open.

For a set \mathcal{S} , let $g_i(\mathcal{S})$ be the image of \mathcal{S} under g_i . We have

$$g_i(\overline{\mathcal{P}_i}) \subseteq \overline{g_i(\mathcal{P}_i)} \subseteq \overline{\prod_{j=1}^7 \mathcal{B}_i^j} \subseteq \prod_{j=1}^7 \overline{\mathcal{B}_i^j}. \quad (3)$$

The first containment in (3) follows from the continuity of g_i , and the second containment follows from $g_i(\mathcal{P}_i) \subseteq \prod_{j=1}^7 \mathcal{B}_i^j$.

The third containment is a property of Cartesian products and closures. arctan2 is Lipschitz on the first, third, fifth, and seventh components of the RHS of (3), and thus is Lipschitz on the corresponding components of $g_i(\overline{\mathcal{P}_i})$ on the LHS. Similarly, \arccos is Lipschitz on the second, fourth, and sixth components of the RHS of (3), and thus is Lipschitz on the corresponding components of $g_i(\overline{\mathcal{P}_i})$. The Lipschitzness of arctan2 and \arccos on their respective components of $g_i(\overline{\mathcal{P}_i})$, combined with the Lipschitzness of g_i on its domain (and thereby $\overline{\mathcal{P}_i}$), implies that MapSample_i , which composes arctan2 and \arccos with g_i , is Lipschitz on $\overline{\mathcal{P}_i}$. Thus, if we let $\mathcal{N}^\# = \prod_{i=1}^{n_{\text{tar}}} \mathcal{P}_i$, MapList is Lipschitz on $\overline{\mathcal{N}^\#} = \prod_{i=1}^{n_{\text{tar}}} \overline{\mathcal{P}_i}$. $\mathcal{N}^\#$ is open since it is the product of open sets. For each $i \in \mathcal{I}$, $v_i^\# \in \mathcal{C}_i$ implies $(h_i^\#, t_i^\#) \in \mathcal{H} \times f_i^{-1}(\mathcal{C}_i)$, and $g_i^{j\#} \in \mathcal{B}_i^j$ implies $(h_i^\#, t_i^\#) \in g_i^{-1} \left(\prod_{j=1}^7 \mathcal{B}_i^j \right)$, so $t_i^\# \in \mathcal{P}_i$. This means $\mathcal{N}^\#$ contains $l_\mathcal{H}^\#$ and is thus nonempty. \square

Next, define the function $\text{ListCost} : \mathcal{L}_\mathcal{H} \rightarrow \mathbb{R}$, which maps a list $l_\mathcal{H}$ to the cost of its associated trajectory.

Lemma 3. (Lipschitz continuity of list costs) Suppose $\mathcal{N} \subseteq \mathcal{L}_\mathcal{H}$ is open and nonempty. Choose \mathcal{N} such that all lists in $\overline{\mathcal{N}}$ have the same corresponding target sequence; Lemma 1 ensures that this choice is always possible. ListCost is Lipschitz on $\overline{\mathcal{N}}$ for the close-enough MT-TSP.

For the robot arm MT-TSP, suppose there is some $l_\mathcal{H}^\# \in \mathcal{N}$ satisfying assumptions (i)-(iii) from Lemma 2. Lemma 2 then guarantees an open set $\mathcal{N}^\#$ such that MapList is Lipschitz on $\overline{\mathcal{N}^\#}$; redefine \mathcal{N} as $\mathcal{N} \cap \mathcal{N}^\#$. ListCost is Lipschitz on $\overline{\mathcal{N}}$ for the robot arm MT-TSP.

For the variable-speed Dubins MT-TSP, for a list $l_\mathcal{H}$, let $(q_{ak-1}, t_{k-1}), (q_{ak}, t_k)$ be the k th consecutive pair of points in the associated tour. Let $v_k^*(l_\mathcal{H}) = v^*(q_{ak-1}, t_{k-1}, q_{ak}, t_k)$, where v^* is defined in Section IV-B. Suppose all $l_\mathcal{H} \in \overline{\mathcal{N}}$ are achieved by trajectories using the same sequence of speeds, i.e. for all $l_\mathcal{H}, l'_\mathcal{H} \in \overline{\mathcal{N}}$, for all k , $v_k^*(l_\mathcal{H}) = v_k^*(l'_\mathcal{H})$. Then ListCost is Lipschitz on $\overline{\mathcal{N}}$ for the variable-speed Dubins MT-TSP.

Proof. Let $l_\mathcal{H} = ((h_1, t_1), (h_2, t_2), \dots, (h_{n_{\text{tar}}}, t_{n_{\text{tar}}})) \in \mathcal{N}$. First, consider the close-enough and robot arm MT-TSPs. ListCost performs the following operations in order:

- 1) Map $l_\mathcal{H}$ to a list $l_{\mathcal{Q}_a} \in \mathcal{L}_{\mathcal{Q}_a}$ via MapList
- 2) Map $l_{\mathcal{Q}_a}$ to a tour Γ by sorting in order of time and prepending $(q_{a,0}, 0)$
- 3) Compute the differences between consecutive configurations in Γ and sum the norms of the differences.

Step 1 is Lipschitz by Lemma 2. Since all lists in $\overline{\mathcal{N}}$ have the same corresponding target sequence, Step 2 is a fixed permutation followed by a prepend operation, which are both affine and thus Lipschitz. Step 3 is a pairwise difference operation, which is linear and thus Lipschitz, followed by an l^2 norm, which is Lipschitz. Since ListCost is a composition of Lipschitz functions, ListCost is Lipschitz on $\overline{\mathcal{N}}$.

Now consider the variable-speed Dubins MT-TSP. ListCost performs steps 1) to 3) above, except in 3), we now sum the values of $v_k^*(l_\mathcal{H})(t_k - t_{k-1})$ for consecutive times t_{k-1}, t_k in Γ . Since we assumed that $v_k^*(l_\mathcal{H})$ is constant on $\overline{\mathcal{N}}$, this summation is linear and thereby Lipschitz in Γ . Since ListCost is a composition of Lipschitz functions, ListCost is Lipschitz on $\overline{\mathcal{N}}$. \square

Theorem 2. (Asymptotic optimality) Suppose $l_\mathcal{H}^*$ is achieved by an optimal $\tau_a^* \in \mathcal{F}$, and let $c^* = \text{ListCost}(l_\mathcal{H}^*)$. Suppose a nonempty open $\mathcal{N} \subseteq \mathcal{L}_\mathcal{H}$ exists satisfying the assumptions of Lemma 3, such that $l_\mathcal{H}^* \in \overline{\mathcal{N}}$. Suppose Assumption 1 holds. As the number of iterations of the loop in Alg. 1 Line 2 tends to infinity, the cost of the returned trajectory converges to c^* with probability 1.

Proof. Let $\epsilon > 0$ be fixed and arbitrary, and let M be the Lipschitz constant of ListCost . Let $\mathcal{B}_{\epsilon/M}(l_\mathcal{H}^*) = \{l_\mathcal{H} \in \mathcal{L}_\mathcal{H} \mid d(l_\mathcal{H}, l_\mathcal{H}^*) < \epsilon/M\}$, and let $\mathcal{D}_{\epsilon/M} = \mathcal{B}_{\epsilon/M}(l_\mathcal{H}^*) \cap \mathcal{N}$. Since $l_\mathcal{H}^* \in \overline{\mathcal{N}}$, $l_\mathcal{H}^*$ is a limit point of \mathcal{N} , which means that every open set containing $l_\mathcal{H}^*$ contains some point in \mathcal{N} distinct from $l_\mathcal{H}^*$. This means $\mathcal{D}_{\epsilon/M}$ is nonempty. Also, $\mathcal{D}_{\epsilon/M}$ is open since it is an intersection of open sets. In the following text, let $\mathbb{P}[E]$ denote the probability of an event E .

Consider an arbitrary loop iteration k . Let $(^k h_i, ^k t_i)$ be the final random sample drawn for target i , and define ${}^k l_\mathcal{H} \in \mathcal{L}_\mathcal{H}$ by ${}^k l_\mathcal{H}[i] = (^k h_i, ^k t_i)$. $\mathcal{D}_{\epsilon/M}$ has positive measure under our sampling distribution by the same argument as Theorem 1,

which means that for some ${}^\epsilon p > 0$, $\mathbb{P}[{}^k l_{\mathcal{H}} \in \mathcal{D}_{\epsilon/M}] = {}^\epsilon p$. If ${}^k l_{\mathcal{H}} \in \mathcal{D}_{\epsilon/M}$, we have the following:

$$|\text{ListCost}({}^k l_{\mathcal{H}}) - {}^* c| \leq M d({}^k l_{\mathcal{H}}, l_{\mathcal{H}}^*) < \epsilon \quad (4)$$

$$\text{ListCost}({}^k l_{\mathcal{H}}) - {}^* c < \epsilon \quad (5)$$

$$\text{ListCost}({}^k l_{\mathcal{H}}) < {}^* c + \epsilon \quad (6)$$

$$\mathbb{P}[\text{ListCost}({}^k l_{\mathcal{H}}) < {}^* c + \epsilon] \geq \mathbb{P}[{}^k l_{\mathcal{H}} \in \mathcal{D}_{\epsilon/M}] = {}^\epsilon p \quad (7)$$

The first inequality in (4) follows from `ListCost` being Lipschitz on \mathcal{N} with Lipschitz constant M , and the second inequality follows from ${}^k l_{\mathcal{H}} \in \mathcal{B}_{\epsilon/M}({}^* l_{\mathcal{H}})$. (5) follows from (4) and the fact that $\text{ListCost}({}^k l_{\mathcal{H}}) - {}^* c \geq 0$ by the optimality of ${}^* c$. (6) adds ${}^* c$ to both sides of (5). (7) follows from the fact that ${}^k l_{\mathcal{H}} \in \mathcal{D}_{\epsilon/M}$ implies (6).

For any iteration l , let ${}^l c$ be the cost of the tour produced, let ${}^l c^*$ be the cost of the optimal tour on the current sample point graph, and let ${}^l Z$ be the event that for all $m \leq l$, ${}^m c > c^* + \epsilon$. (7), along with the independence of ${}^k l_{\mathcal{H}}$ from ${}^{k-1} Z$, implies

$$\mathbb{P}[\text{ListCost}({}^k l_{\mathcal{H}}) < c^* + \epsilon | {}^{k-1} Z] \geq {}^\epsilon p \quad (8)$$

$$\mathbb{P}[{}^k c^* < c^* + \epsilon | {}^{k-1} Z] \geq {}^\epsilon p. \quad (9)$$

Also, since `TourViaGTSP` attempts to randomly sample an optimal tour after running PGLNS,

$$\mathbb{P}[{}^k c = {}^k c^* | {}^{k-1} Z] \geq \frac{1}{n_{\text{tar}}!} \left(\frac{1}{n_{\text{rand}} + 1} \right)^{n_{\text{tar}}}. \quad (10)$$

In (10), $\frac{1}{n_{\text{tar}}!}$ is the probability of selecting the optimal sequence of targets using uniform random sampling, and $\left(\frac{1}{n_{\text{rand}} + 1} \right)^{n_{\text{tar}}}$ is the probability of randomly selecting the optimal node in each target's cluster using uniform random sampling. Denote the RHS of (10) as \underline{p} . (9) and (10) imply $\mathbb{P}[{}^k c < c^* + \epsilon | {}^{k-1} Z] \geq {}^\epsilon p \underline{p} > 0$. This means

$$\mathbb{P}[{}^k c > c^* + \epsilon | {}^{k-1} Z] \leq 1 - {}^\epsilon p \underline{p}. \quad (11)$$

Denote the RHS of (11) as ζ . Since ${}^k Z = ({}^k c > c^* + \epsilon) \cap {}^{k-1} Z$, Bayes' rule tells us that

$$\mathbb{P}[{}^k Z] = \mathbb{P}[{}^k c > c^* + \epsilon | {}^{k-1} Z] \mathbb{P}[{}^{k-1} Z] \leq \zeta \mathbb{P}[{}^{k-1} Z] \quad (12)$$

where the second inequality follows from (11). Now we show by induction that $\mathbb{P}[{}^k Z] \leq \zeta^k$. As the base case, let $k = 1$. Since $k - 1 = 0$, there is no iteration $k - 1$, so ${}^{k-1} Z$ is vacuously true and $\mathbb{P}[{}^{k-1} Z] = 1$. Applying (12), $\mathbb{P}[{}^1 Z] \leq \zeta^1$. As our induction hypothesis, for some $k > 1$, suppose

$$\mathbb{P}[{}^{k-1} Z] \leq \zeta^{k-1}. \quad (13)$$

For our induction step, we substitute (13) into (12) and obtain $\mathbb{P}[{}^k Z] \leq \zeta^k$, which proves $\mathbb{P}[{}^k Z] \leq \zeta^k$ for all k .

Note that ${}^k Z \iff {}^k c > c^* + \epsilon$. This is because in IRG-PGLNS, tour cost never increases from one iteration to the next, so ${}^k c > c^* + \epsilon$ is only possible if ${}^m c > c^* + \epsilon$ for all $m \leq k$. Thus, $\mathbb{P}[{}^k c > c^* + \epsilon] \leq \zeta^k$. Combining this with $\zeta < 1$ (implied by ${}^\epsilon p \underline{p} > 0$), we have $\sum_{k=1}^{\infty} \mathbb{P}[{}^k c > c^* + \epsilon] < \infty$.

Equivalently, $\sum_{k=1}^{\infty} \mathbb{P}[{}^k c - c^* > \epsilon] < \infty$. The optimality of c^*

implies ${}^k c - c^* \geq 0$, so $\sum_{k=1}^{\infty} \mathbb{P}[|{}^k c - c^*| > \epsilon] < \infty$. The Borel-Cantelli Lemma [65] then implies $\mathbb{P}[\limsup_{k \rightarrow \infty} |{}^k c - c^*| > \epsilon] = 0$, i.e. ${}^k c$ converges to c^* almost surely. By Assumption 1, the returned trajectory's cost converges to c^* almost surely. \square

VII. NUMERICAL RESULTS

We ran experiments on an Intel i9-9820X 3.3GHz CPU with 128 GB RAM and 10 cores. Section VII-A describes how we generate problem instances, and Section VII-B describes how we tune the planners under comparison. In Sections VII-C to VII-G, we compare IRG-PGLNS and PCG to a baseline and two ablations. Our baseline for the close-enough MT-TSP and variable-speed Dubins MT-TSP is a modification of the memetic algorithm [15], which addresses the fixed-speed Dubins close-enough MT-TSP without time windows. In particular, we extend [15] to handle time windows, we specialize [15] to the close-enough MT-TSP and variable-speed Dubins MT-TSP, and we parallelize [15]. Details of these modifications are in Appendix A. We do not run this baseline for the robot arm MT-TSP, since [15] did not consider a robot arm. Our first ablation, IRG-GLNS, is the same as IRG-PGLNS except that IRG-GLNS uses GLNS instead of PGLNS as the GTSP solver. Our second ablation, called Parallel Decoupled GTSPs (PDG), is essentially an ablation of PCG where the processes do not communicate. PDG runs Alg. 1 Line 1, then spawns several parallel child processes, each running Lines 2-5 and updating its own copy of Γ^* . When the planning time budget is reached, PDG returns the best Γ^* over all child processes. This strategy is referred to as independent multi-search in the parallel metaheuristics literature [66]. Both IRG-GLNS and PDG fall into the IRG framework.

The optimal solutions for the problem instances in Sections VII-C to VII-G are unknown, since there are no optimal solvers for the close-enough, variable-speed Dubins, and robot arm MT-TSPs. To evaluate how close IRG-PGLNS and PCG come to the optimum, in Section VII-H, we generate a set of instances for what we call the *linear MT-TSP*, i.e. the MT-TSP from Fig. 1 (a), but targets move along straight-line paths with constant velocity. Optimal solutions for the linear MT-TSP can be found using [19]. In Section VII-H, we show that IRG-PGLNS and PCG converge closely to the optimum on instances where we can find the optimum, and that they scale better to larger numbers of targets than the optimal solver. Finally, in Section VII-I, we evaluate the IRG framework's method of solving the GTSP on its first set of sample points, showing that IRG's method finds feasible solutions more quickly than existing GTSP algorithms.

Each planner was given a 30 s time budget per instance for the close-enough MT-TSP and a 1 minute time budget per problem instance in the variable-speed Dubins and robot arm MT-TSPs. We used a shorter time budget for the close-enough MT-TSP because sampling and edge cost computations are relatively inexpensive, and all planners tend to converge more quickly than in the other two variants. When constructing the sample point graph, IRG-PGLNS and IRG-GLNS invoked `TrajExists` for different node pairs in parallel using 10

threads. Additionally, for the robot arm MT-TSP, to mitigate the computational expense of inverse kinematics during sampling, IRG-GLNS and IRG-PGLNS generated points for different targets in parallel using 10 processes, i.e. they parallelized the loop on Line 3 of Alg. 1. PCG and PDG, on the other hand, iterated over targets serially, since they already sample several different sets of points for each target in parallel. When generating an initial tour using Alg. 2, we parallelize the edge cost computations when constructing the sample point graph for all MT-TSP variants, parallelize the sampling for the robot arm MT-TSP, and generate successors for search nodes in parallel during the DFS.

A. Generating Problem Instances

We first generated 20 instances for each problem variant, which we call *default* instances, using *default* parameter values specified for each variant in Sections VII-A2-VII-A3. The default number of targets is 200 for all variants. We then varied parameters within the default instances to generate additional instances. For each default instance, we sampled an initial agent configuration $q_{a,0}$ uniformly at random from a set $\mathcal{Q}_{a,0}$, specified for each variant in Sections VII-A2-VII-A3. To generate trajectories of targets such that each instance was feasible, we extended the method from [67]. We first generated a random feasible tour, $((q_{a,0}, 0), (q_{a,1}, t_1), \dots (q_{a,n_{\text{tar}}}, t_{n_{\text{tar}}}))$, as well as a random, two-segment piecewise-linear trajectory $\tilde{\tau}_i$ for each $i \in \mathcal{I}$ that passed through $(q_{a,i}, t_i)$. Then for each $i \in \mathcal{I}$, we fit a cubic B-spline that passed through $(q_{a,i}, t_i)$ and the endpoints of the segments of $\tilde{\tau}_i$ to obtain the final trajectory τ_i . Instance generation code is provided in the multimedia attachment.

1) *Close-Enough MT-TSP*: For the close-enough MT-TSP, $\mathcal{Q}_{a,0} = [-50 \text{ m}, 50 \text{ m}]^2$. The agent's speed limit was 5 m/s in all instances. All targets had time windows of length 108 s. Each segment of $\tilde{\tau}_i$ had a direction sampled uniformly at random and a speed uniformly random sampled from the range [0.5, 1] m/s. Within a single instance, all targets have a common radius value, which we call the *target radius*. The default target radius was 12 m.

2) *Variable-Speed Dubins MT-TSP*: For the variable-speed Dubins MT-TSP, $\mathcal{Q}_{a,0} = [-50 \text{ m}, 50 \text{ m}]^2 \times \mathbb{S}^1$. The agent's default v_{\min} was 2 m/s. In all instances, $v_{\max} = 5 \text{ m/s}$ and $\omega_{\max} = 0.25 \text{ rad/s}$. We let $\mathcal{S}_{\text{speed}} = \{v_{\min}, \frac{2}{3}v_{\min} + \frac{1}{3}v_{\max}, \frac{1}{3}v_{\min} + \frac{2}{3}v_{\max}, v_{\max}\}$. All targets had time windows of length 108 s. Each segment of $\tilde{\tau}_i$ had a direction sampled uniformly at random and a speed uniformly random sampled from the range [0.5, 1] m/s.

3) *Robot Arm MT-TSP*: For the robot arm MT-TSP, we generated instances for a 7 DOF arm with the same geometry and joint angle limits as the KUKA iiwa, and we set $\mathcal{Q}_{a,0} = \mathcal{Q}_a$. All joints had a default max speed of 5 rad/s. All targets had time windows of length 3 s. Each segment of $\tilde{\tau}_i$ necessarily had a position component and orientation component. Each position component had a direction sampled uniformly at random and a speed uniformly random sampled from the range [0.5, 1] m/s. Each orientation component had a world-frame angular velocity whose x , y , and z components were each sampled from the standard normal distribution.

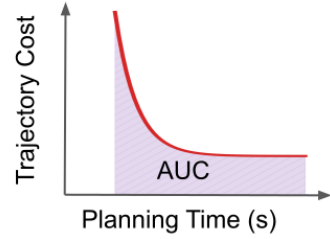


Fig. 4. Performance metric: area under the curve (AUC). Small AUC is desirable, as it indicates fast convergence to a low-cost solution.

B. Tuning the Planners

We tuned three values for each IRG-based planner for each problem variant: $n_{\text{rand, init}}$, used in Alg. 2, n_{rand} , used in Alg. 1 and Alg. 6, and n_{term} , used in Alg. 5. GLNS and PGLNS have other tunable parameters, which we set equal to their fast mode values [16].

1) *Tuning $n_{\text{rand, init}}$* : $n_{\text{rand, init}}$ is common to all planners within a problem variant, since they all use the same initial tour generation routine. We determined $n_{\text{rand, init}}$ by first generating a set of 30 tuning instances using default parameters, except we set the target radius to zero in the close-enough MT-TSP, $v_{\min} = 5$ in the variable-speed Dubins MT-TSP, and $v_{\max} = 4.1$ for the robot arm MT-TSP, to ensure that the initial tour generation was tuned for the most constrained instances. We used a different set of random seeds for generating the tuning instances than the instances in later sections, so that none of the tuning instances are used in subsequent experiments.

For each variant, we ran `GenerateInitialTour` on the tuning instances, setting $n_{\text{rand, init}} = 2$. After finding a tour for all 30 instances, we set $n_{\text{rand, init}}$ equal to the largest final value of $|\mathcal{S}_1|$ over all instances for that variant. The tuned $n_{\text{rand, init}}$ values for the close-enough MT-TSP, variable-speed Dubins MT-TSP, and robot arm MT-TSP were 8, 42, and 32, respectively.

2) *Tuning n_{rand} and n_{term}* : To tune n_{rand} and n_{term} , we generated another set of 10 tuning instances per problem variant using default parameters. Using the same strategy as [16], we set $n_{\text{term}} = \alpha_{\text{term}} n_{\text{cluster}}$, where n_{cluster} is the number of clusters in the GTSP. In all GTSPs we solved, $n_{\text{cluster}} = n_{\text{tar}} + 1$, since we have a cluster for each target and a singleton cluster containing $(q_{a,0}, 0)$. For each planner and problem variant, we ran the planner until the time budget on each tuning instance, for each combination of $n_{\text{rand}} \in \{1, 2, 4, 8, 16, 32, 64\}$ and $\alpha_{\text{term}} \in \{1, 2, 4, 8, 16, 32, 64\}$. For each instance and parameter setting, we recorded the solution cost vs. planning time, then computed the area under the curve (AUC) of the cost vs. planning time curve, as visualized in Fig. 4. We chose the combination of n_{rand} and n_{term} that minimized the median AUC over the 10 tuning instances. We show the tuned n_{rand} and α_{term} values in Tables I and II, respectively.

For all planners, the tuned value of α_{term} is smaller than the original value of 60 in GLNS fast mode, except for IRG-PGLNS in the variable-speed Dubins MT-TSP. The smaller α_{term} leads planners to resample more frequently and spend less time solving any particular GTSP than if they were using the original α_{term} from GLNS's fast mode. GLNS's default

TABLE I
TUNED VALUES OF n_{rand}

	Close-Enough MT-TSP	Variable-Speed Dubins MT-TSP	Robot Arm MT-TSP
IRG-GLNS (ablation)	32	32	32
PDG (ablation)	8	2	32
IRG-PGLNS	16	32	32
PCG	16	4	16

TABLE II
TUNED VALUES OF α_{term}

	Close-Enough MT-TSP	Variable-Speed Dubins MT-TSP	Robot Arm MT-TSP
IRG-GLNS (ablation)	4	16	8
PDG (ablation)	1	4	8
IRG-PGLNS	4	64	8
PCG	4	8	4

and slow modes have $\alpha_{\text{term}} = 60$ and 150, respectively, and thus the tuned values are often smaller than the α_{term} for all of GLNS’s solver modes.

3) *Tuning the Memetic Algorithm Baseline*: As described in Appendix A, the memetic algorithm baseline, based on [15], performs several iterations, where each iteration performs operations on a population of solutions to generate a new population. We use the algorithm parameters from [15], except for the population size, since we found that in instances with 200 targets, the algorithm would spend most of its time constructing its initial population and little time improving the solutions in the population. [15] did not have this issue because they only tested instances with up to 40 targets, and they did not consider time windows. Time windows make generating an initial population more computationally expensive, as discussed in Appendix A. Therefore, we tune the population size as follows.

Using the same strategy as [15], we set the population size equal to $\alpha_{\text{pop}} n_{\text{tar}}$ and tuned α_{pop} . For the close-enough MT-TSP, we ran the baseline until the time budget on each tuning instance with $\alpha_{\text{pop}} \in \{0.01, 0.1, 1, 10\}$, then chose the α_{pop} that minimized the median AUC. We did the same for the variable-speed Dubins MT-TSP, but with $\alpha_{\text{pop}} \in \{0.01, 0.02, 0.03, 0.04\}$. We chose the set of attempted α_{pop} values for each variant so that the largest attempted α_{pop} resulted in the entire time budget being spent initializing the population for 200 targets. The tuned α_{pop} values were 0.1 for the close-enough MT-TSP and 0.04 for the variable-speed Dubins MT-TSP.

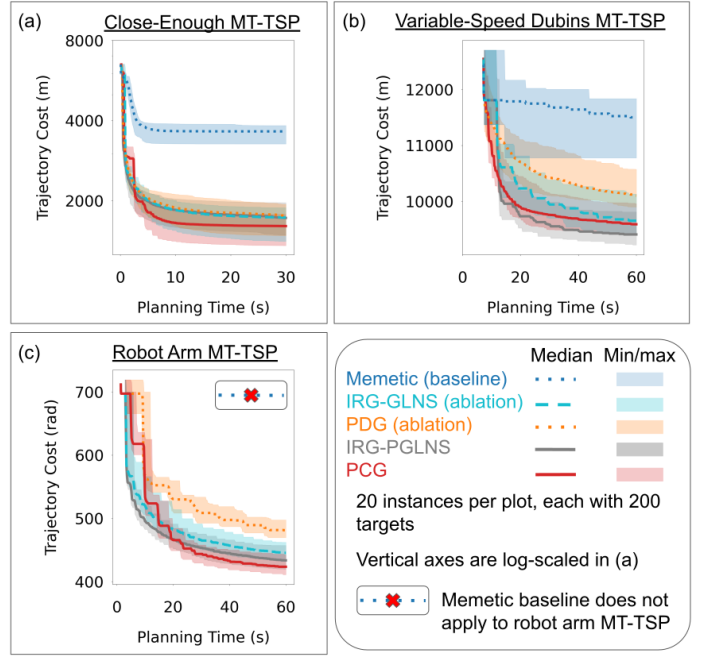


Fig. 5. Cost vs. time for three MT-TSP variants, in instances with 200 targets. IRG-PGLNS and PCG find notably lower-cost solutions than the baseline and ablations, except for the close-enough MT-TSP (a), where IRG-PGLNS outperforms the memetic baseline while performing similarly to the ablations.

C. Varying the Number of Targets

In this experiment, we varied the number of targets from 50 to 200 for all problem variants, with other instance parameters at their default values. The AUC values for all numbers of targets are given in Tables III-V, and the cost vs. time curves for 200 targets are shown in Fig. 5. All of the IRG-based planners outperform the memetic algorithm in min, median, and max AUC. For the close-enough MT-TSP, PCG has the smallest median AUC for all numbers of targets (Table III). In the variable-speed Dubins MT-TSP, IRG-PGLNS has the smallest median AUC for all numbers of targets (Table IV). Finally, for the robot arm MT-TSP, IRG-PGLNS has the smallest median AUC for 100 or more targets (Table V).

The memetic algorithm performs poorly largely due to the greedy optimization it uses to compute an agent trajectory for any fixed sequence of targets, i.e. the “transformation” procedure described in Appendix A. We have found that this procedure often fails to generate feasible trajectories in the presence of time windows. The reason PCG noticeably outperforms IRG-PGLNS in the close-enough MT-TSP, but not for the other variants, is that parallelizing operations on a single sample point graph (sampling, computing edge costs, and solving a GTSP), as IRG-PGLNS does, yields smaller reductions in median iteration time for the close-enough MT-TSP than in the other variants. Section VII-D discusses this further.

D. Varying the Number of Cores

In this experiment, we varied the number of cores used by the IRG-based algorithms and the memetic baseline. For IRG-GLNS, the number of cores is the number of threads used for edge cost computations, as well as the number of

TABLE III

AUC ($m \cdot s$) IN THOUSANDS FOR THE CLOSE-ENOUGH MT-TSP. ENTRIES ARE SHOWN AS MIN|MEDIAN|MAX. BEST MIN, MEDIAN, AND MAX IN EACH COLUMN ARE BOLDED. STATISTICS ARE TAKEN OVER 20 INSTANCES FOR EACH NUMBER OF TARGETS.

	$n_{tar} = 50$	$n_{tar} = 100$	$n_{tar} = 150$	$n_{tar} = 200$
Memetic (baseline)	18.8 26.2 30.7	47.8 54.4 60.8	74.0 82.4 95.5	103 112 119
IRG-PGLNS (ablation)	8.92 14.0 16.9	21.2 25.9 32.0	35.2 39.8 46.1	48.7 57.3 61.9
PDG (ablation)	8.62 13.5 15.9	20.9 25.6 32.3	36.1 40.2 46.0	49.6 58.5 64.2
IRG-PGLNS	8.69 13.8 16.7	21.9 26.3 31.8	34.7 40.4 50.0	49.1 56.6 62.2
PCG	8.62 12.5 16.5	19.3 24.2 30.5	32.4 37.4 43.0	46.0 53.6 58.4

TABLE IV

AUC (s^2) IN THOUSANDS FOR THE VARIABLE-SPEED DUBINS MT-TSP. ENTRIES ARE SHOWN AS MIN|MEDIAN|MAX. BEST MIN, MEDIAN, AND MAX IN EACH COLUMN ARE BOLDED. STATISTICS ARE TAKEN OVER 20 INSTANCES FOR EACH NUMBER OF TARGETS.

	$n_{tar} = 50$	$n_{tar} = 100$	$n_{tar} = 150$	$n_{tar} = 200$
Memetic (baseline)	138 155 188	319 337 348	450 481 505	570 613 630
IRG-PGLNS (ablation)	128 138 144	256 271 282	399 411 423	517 533 554
PDG (ablation)	134 143 150	273 288 299	413 428 452	538 552 579
IRG-PGLNS	128 138 145	257 269 281	388 398 415	505 513 535
PCG	133 140 150	262 276 288	391 408 426	509 520 544

TABLE V

AUC ($rad \cdot s$) IN THOUSANDS FOR TGE ROBOT ARM MT-TSP. ENTRIES ARE SHOWN AS MIN|MEDIAN|MAX. BEST MIN, MEDIAN, AND MAX IN EACH COLUMN ARE BOLDED. STATISTICS ARE TAKEN OVER 20 INSTANCES FOR EACH NUMBER OF TARGETS.

	$n_{tar} = 50$	$n_{tar} = 100$	$n_{tar} = 150$	$n_{tar} = 200$
IRG-PGLNS (ablation)	5.87 6.39 6.91	12.4 13.2 13.9	19.8 20.4 21.2	27.5 28.1 28.8
PDG (ablation)	6.26 6.78 7.12	13.8 14.4 14.9	21.8 22.5 23.3	30.4 31.0 31.6
IRG-PGLNS	6.01 6.45 6.78	12.6 13.2 13.7	19.4 20.1 20.9	26.5 27.4 28.6
PCG	6.03 6.47 6.88	12.5 13.3 13.5	19.5 20.2 21.1	27.0 27.7 28.4

processes used for sampling in the robot arm MT-TSP. For PDG and PCG, the number of cores is n_{proc} . For IRG-PGLNS, the number of cores is the number of threads used for edge cost computations, the number of processes used for sampling in the robot arm MT-TSP, and n_{thread} in PGLNS. For the memetic algorithm, the number of cores is the number of threads used in initial population construction and when generating a new population from a previous one (see Appendix A).

For each algorithm, the first time that Alg. 2 is invoked, we use all the cores on our computer, so that the initial solution is found at approximately the same time in all experiments. This avoids counterintuitive trends where using fewer cores causes the initial solution computation to finish later and the AUC to decrease, which would give an impression that using fewer cores improves performance. In the IRG-based algorithms, Alg. 2 is only called once, whereas in the memetic baseline, Alg. 2 is called once for each member of the initial population; therefore, the memetic baseline uses all cores to generate its first population member, then n_{core} cores to generate subsequent ones.

First, to elucidate why IRG-PGLNS underperformed PCG for the close-enough MT-TSP in Section VII-C, we plot each component of IRG-PGLNS's computation time per iteration in Fig. 6. The total speedup when going from 1 to 10 cores is small for the close-enough MT-TSP when compared to the variable-speed Dubins and robot arm MT-TSPs, making it more useful to consider several sample point graphs at once, as PCG does, rather than applying parallelization to a single sample point graph, as IRG-PGLNS does. The reason that IRG-PGLNS has a small total speedup for the close-enough MT-TSP is that computing edge costs, which is embarrassingly parallel, is less expensive than solving the GTSP, which is not embarrassingly parallel, as shown in Fig. 6 (a). In all the variants, parallelizing the GTSP solve tends to provide sublinear speedups, and thus in the close-enough MT-TSP, where the GTSP solve is the bottleneck, the overall speedup for IRG-PGLNS is small. Meanwhile, in the variable-speed Dubins MT-TSP, the bottleneck is computing edge costs (Fig. 6 (b)), and in the robot arm MT-TSP, the bottleneck is sampling (Fig. 6 (c)). Both of these bottlenecks are embarrassingly parallel, and parallelizing them leads to large reductions in computation time, leading IRG-PGLNS to perform well on the variable-speed Dubins and robot arm MT-TSPs.

Next, we examine the AUC for all planners as we vary the number of cores in Fig. 7. For all planners and problem variants, except for PDG, AUC tends to decrease with the number of cores used. PDG's displays little trend with respect to the number of cores used, highlighting the importance of communication between processes in PCG.

E. Close-Enough MT-TSP: Varying the Target Radius

In this experiment, we varied the target radius in the close-enough MT-TSP from 0 to 12 m, leaving other instance parameters at their default values. The results are in Fig. 8 (a). As the target radius becomes larger, the AUCs become smaller for all planners, since the instances become less constrained and have smaller optimal costs. For all target radii, PCG has the smallest min, median, and max AUC.

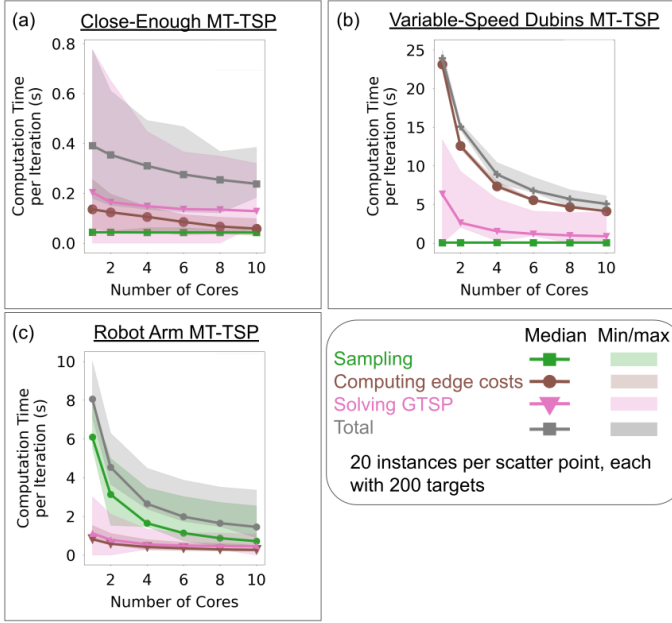


Fig. 6. Components of runtime per iteration of IRG-PGLNS as we vary the number of cores it uses. (a) In the close-enough MT-TSP, solving the GTSP is the bottleneck, and increasing the number of cores from 1 to 10 provides a 1.6x reduction in median GTSP solve time per iteration. (b) In the variable-speed Dubins MT-TSP, computing edge costs is the bottleneck, and increasing the number of cores from 1 to 10 provides 5.6x reduction in median edge cost computation time per iteration. (c) In the robot arm MT-TSP, sampling is the bottleneck, and increasing the number of cores from 1 to 10 provides an 8.5x reduction in median sampling time per iteration.

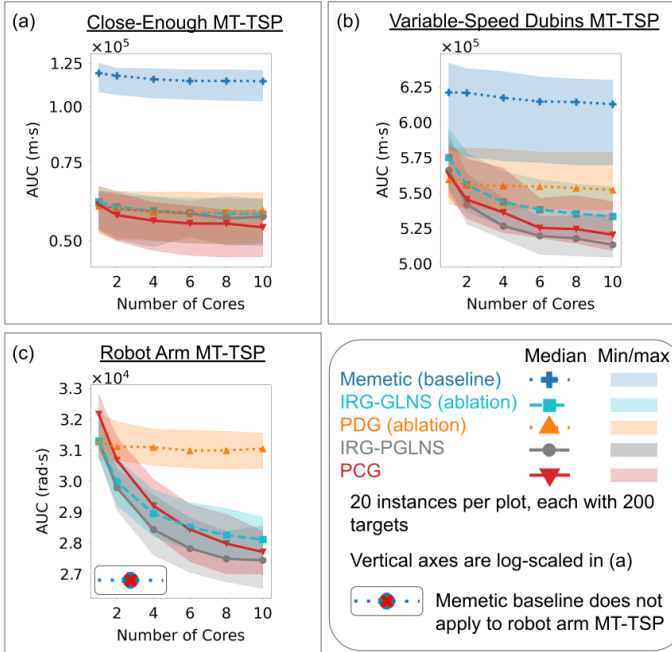


Fig. 7. Varying the number of cores used by each algorithm. Methods' AUC values differ when they all use 1 core because they use different values of n_{rand} and α_{term} . All planners' AUC values tend to decrease as we increase the number of cores. The decreases for PDG and the memetic algorithm are smaller than for other planners.

F. Variable-Speed Dubins MT-TSP: Varying the Minimum Speed

In this experiment, we varied the agent's minimum speed v_{\min} in the variable-speed Dubins MT-TSP from 2 m/s to 5 m/s, leaving other instance parameters at their default values. When $v_{\min} = 5$, v_{\min} equals v_{\max} , and thus we have a fixed-speed Dubins MT-TSP. The results are in Fig. 8 (b). As v_{\min} becomes larger, the median AUC becomes larger for all planners, since the instances become more constrained and have higher optimal costs. Counterintuitively, the minimum AUC drops when increasing v_{\min} from 4 to 5. The small minimum AUC for $v_{\min} = 5$ is due to the initial tour generation taking a large time in two instances, since it exhausted its initial sample point graph without finding a tour and needed to add more sample points. This led to the cost vs. time curve beginning at a later time, but ending at the same fixed time budget as in other instances, thus having smaller AUC.

Planners' AUC values tend to become more similar as we increase v_{\min} . This is expected, since the gap in minimum and maximum possible trajectory cost becomes smaller as v_{\min} approaches v_{\max} . That is, if the latest starting time window begins at \underline{t} , and the latest ending time window begins at \bar{t} , the minimum possible cost for an instance is $\underline{c} = v_{\min}\underline{t}$, and the maximum possible cost is $\bar{c} = v_{\max}\bar{t}$. As we increase v_{\min} , \underline{c} becomes closer to \bar{c} .

G. Robot Arm MT-TSP: Varying the Max Joint Speed

In this experiment, we varied the arm's max joint speed in the robot arm MT-TSP from 4.1 rad/s to 5.0 rad/s, leaving other instance parameters at their default values. The results are in Fig. 8 (c). As v_{\max} increases, the median AUC tends to decrease for all planners, since the instances become less constrained and have smaller optimal costs. IRG-PGLNS has the smallest min and median AUC for all values of v_{\max} . All planners' minimum AUCs are unusually small for $v_{\max} = 4.1$ for the same reason that the minimum AUCs were unusually small in the variable-speed Dubins MT-TSP with $v_{\min} = 5$: there was an instance where the initial tour generation increased its number of sample points and thus took an excessively long time.

H. Linear MT-TSP: Evaluating Asymptotic Optimality

In this section, we evaluate how quickly IRG-PGLNS and PCG converge to the optimal cost for the linear MT-TSP, as defined in the beginning of Section VII. In particular, we generated instances with 10 to 40 targets using Steps 1 to 5 described in Section VII-A, but we replaced the two-segment piecewise-linear trajectories with single-segment trajectories. Also, instead of generating τ_i by fitting a B-spline to $\tilde{\tau}_i$, we simply set $\tau_i = \tilde{\tau}_i$. The instances used the same parameters as the instances for the close-enough MT-TSP, except we made the time window length 54 s rather than 108 s so that we could find the optimum using the optimal MICP [19] for up to 20 targets within a 1 minute time budget. We then ran the optimal MICP, IRG-PGLNS, and PCG on each instance for 1 minute. For IRG-PGLNS and PCG, we modified the PGLNS

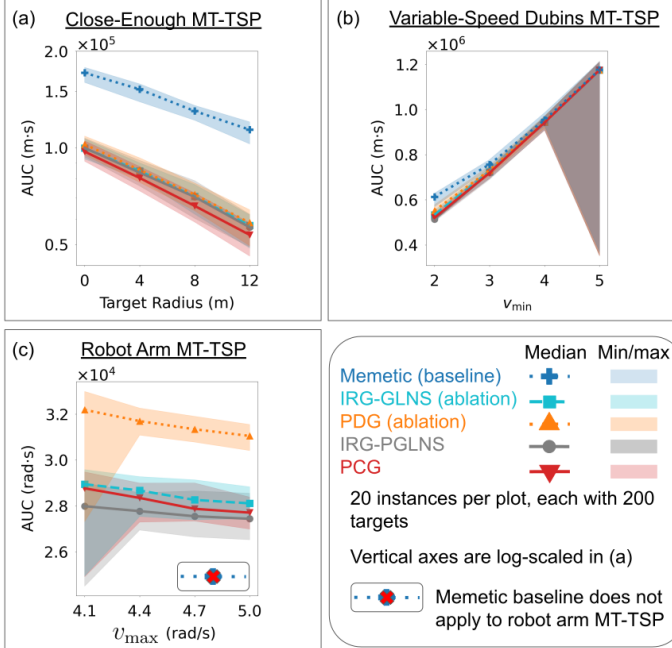


Fig. 8. (a) Varying the target radius for the close-enough MT-TSP. PCG has smaller min, median, and max AUC than all other planners for all radii. (b) Varying the agent's minimum speed for the variable-speed Dubins MT-TSP. IRG-PGLNS and PCG perform similarly to each other and have smaller median and max AUC than baselines and ablations for $v_{\min} \leq 4$. (c) Varying the max joint speeds for the robot arm MT-TSP. IRG-PGLNS has smaller min and median AUC than all other planners for all v_{\max} values.

TABLE VI
PERCENT OF INSTANCES WITH OPTIMAL TARGET SEQUENCE RETURNED

	$n_{\text{tar}} = 10$	$n_{\text{tar}} = 20$
IRG-PGLNS	95%	55%
PCG	90%	70%

and GLNS solvers by allowing the solvers to remove up to $n_{\text{cluster}} - 1$ nodes from a tour in each iteration, as opposed to the maximum of $0.1n_{\text{cluster}}$ removals used in GLNS fast mode. We did so because we found that for small numbers of clusters, only allowing $0.1n_{\text{cluster}}$ removals led to convergence to notably suboptimal solutions. We did not make this change for other experiments because we found that for 100 or more targets, allowing $n_{\text{cluster}} - 1$ removals did not provide significant benefit.

The results are in Fig. 9. The optimal MICP certified that it found the optimal solution in all instances with 10 to 20 targets, but not in any instance with 30 to 40 targets. IRG-PGLNS and PCG both converged to solutions of similar quality to the optimal MICP. In Table VI, we show that in the majority of 10 and 20 target instances, IRG-PGLNS and PCG actually returned the optimal sequence of targets.

I. Evaluating Initial Tour Generation

In this section, we evaluate the effectiveness of the DAG-DFS in Alg. 4 for solving the GTSP in Alg. 2, when generating the initial tour in IRG. All methods we compare against run Alg. 2, but use a different method of solving the GTSP. The first method we compare against, which we call ‘‘Integer

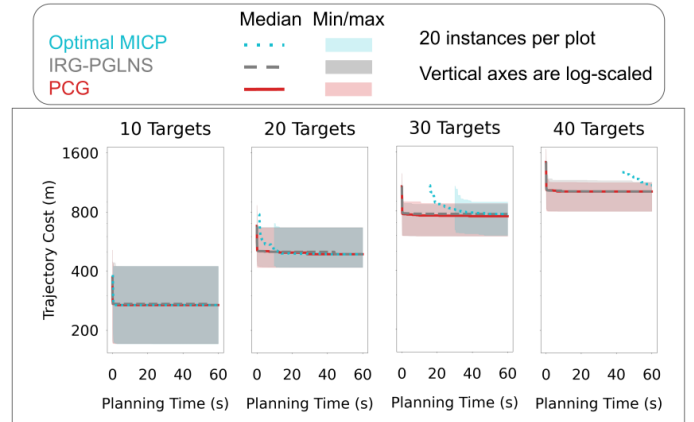


Fig. 9. Testing IRG variations against optimal MICP solver [19] on ‘‘linear’’ MT-TSP instances, as defined at the beginning of Section VII. For instances with 10 and 20 targets, the optimal MICP found the optimal solution within the 1 min time limit, but on the instances with 30 and 40 targets, it did not certify that it found the optimum in any instance. IRG-PGLNS and PCG converge closely to the optimum for 10 and 20 targets and scale better with the number of targets than the optimal MICP.

Program,’’ is a baseline that solves the GTSP using an integer program [68]. The second method, which we refer to as ‘‘GLNS,’’ is a baseline that solves the GTSP using GLNS [16]. The third method, which we refer to as ‘‘PGLNS,’’ solves the GTSP using PGLNS. The fourth method, which we call ‘‘DAG-DFS-no-prune,’’ is an ablation that solves the GTSP using the DAG-DFS (Alg. 4), but without using the BEFORE sets for pruning. Finally, DAG-DFS uses Alg. 4 without modification. Each method was given a time limit of 30 s for the close-enough MT-TSP and a limit of 60 s for the variable-speed Dubins and robot arm MT-TSPs, matching the time limits in the previous experiments. All methods stop as soon as they find a feasible solution.

In Section IV-B, we set the cost of infeasible edges for GLNS and PGLNS using the cost of the best tour generated so far. Since we do not have a best tour for this experiment—the purpose of the experiment is to test methods of generating an initial tour—we set the infeasible edge costs equal to $(n_{\text{tar}} + 1)\bar{c}$, where \bar{c} is the largest feasible edge cost, scaled and rounded as in Section IV-B. Since we do not have a seed tour to pass GLNS or PGLNS, we use a ‘‘random insertion tour,’’ as described in [16]. If GLNS or PGLNS reaches its termination criteria without finding a feasible tour, and there is time left, we restart the algorithm with a new random insertion tour.

We used the tuned $n_{\text{rand},\text{init}}$ values for each variant MT-TSP stated in Section VII-B, and the number of points never needed to be increased in Alg. 2 after generating the initial set of samples. For GLNS and PGLNS, we used the parameters from GLNS’s fast mode. The results are in Fig. 10. Our DAG-DFS method tends to find initial solutions more quickly than the other methods, particularly for large numbers of targets. Comparisons against DAG-DFS-no-prune show that pruning based on the BEFORE sets is key to achieving low runtimes.

In Fig. 11, we plot the costs of the solutions found by each method. The baselines tend to find solutions with smaller median cost than DAG-DFS when the number of targets is small enough that the baselines actually find solutions. A

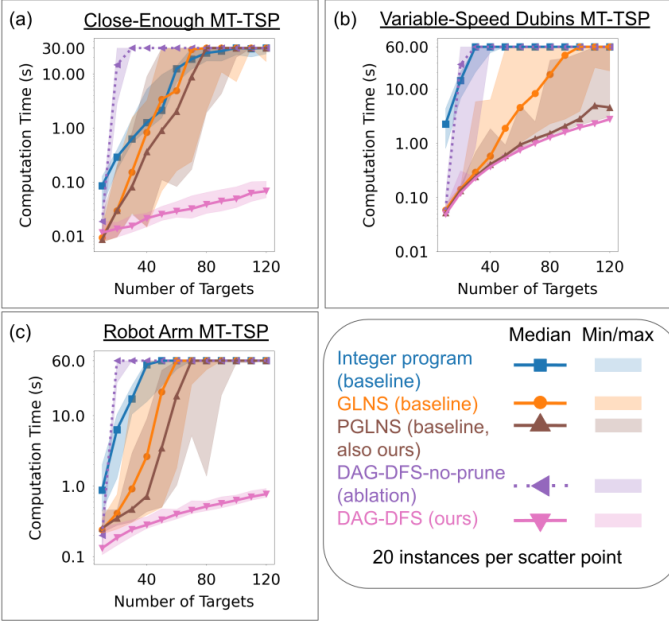


Fig. 10. Comparison of computation time for methods for solving the GTSP on the first set of sample points. Our DAG-DFS method, used in all the IRG variants, scales better with the number of targets than the other methods.

notable exception is in Fig. 11 (a), where the median cost for the Integer Program baseline is larger than the other methods', including DAG-DFS, for 50 or fewer targets. Integer Program's cost then drops sharply when we increase the number of targets from 50 to 60. In Fig. 10 (a), this drop is accompanied by a sharp rise in computation time. These sharp changes occur due to a sharp increase in the amount of time the integer program solver Gurobi spends adding cutting planes and tightening its root relaxation before eventually finding a feasible solution using one of its heuristics. While the internals of Gurobi are proprietary, we attribute this sharp increase to Gurobi switching to a heuristic that takes longer and thus indirectly benefits from a tighter relaxation.

VIII. CONCLUSION

In this paper, we introduced the IRG framework for variants of the MT-TSP, as well as two parallel algorithms in this framework: IRG-PGLNS and PCG. We proved our algorithms' probabilistic completeness and asymptotic optimality, and we demonstrated their ability to quickly find high-quality solutions compared to a baseline and two ablations. One direction for future work is to apply IRG to variants of the MT-TSP with obstacles [67], [69]. When obstacles are present, evaluating the edge costs in IRG's sample point graphs will become even more of a bottleneck, motivating the use of lazy edge evaluation methods [70] and methods of reusing computation effort between evaluations of different edges' costs [71].

REFERENCES

- [1] W. J. Cook, D. L. Applegate, R. E. Bixby, and V. Chvatal, *The traveling salesman problem: a computational study*. Princeton university press, 2011.
- [2] G. Gutin and A. P. Punnen, *The traveling salesman problem and its variations*. Springer Science & Business Media, 2006, vol. 12.
- [3] J. W. Barnes, V. D. Wiley, J. T. Moore, and D. M. Ryer, "Solving the aerial fleet refueling problem using group theoretic tabu search," *Mathematical and computer modelling*, vol. 39, no. 6-8, pp. 617–640, 2004.
- [4] I. Granado, L. Hernando, Z. Uriondo, and J. A. Fernandes-Salvador, "A fishing route optimization decision support system: The case of the tuna purse seiner," *European Journal of Operational Research*, vol. 312, no. 2, pp. 718–732, 2024.
- [5] C. Groba, A. Sartal, and X. H. Vázquez, "Solving the dynamic traveling salesman problem using a genetic algorithm with trajectory prediction: An application to fish aggregating devices," *Computers & Operations Research*, vol. 56, pp. 22–32, 2015.
- [6] G. G. Brown, W. C. DeGrange, W. L. Price, and A. A. Rowe, "Scheduling combat logistics force replenishments at sea for the us navy," *Naval Research Logistics (NRL)*, vol. 64, no. 8, pp. 677–693, 2017.
- [7] D. Marlow, P. Kilby, and G. Mercer, "The travelling salesman problem in maritime surveillance—techniques, algorithms and analysis," in *Proceedings of the international congress on modelling and simulation*. Citeseer, 2007, pp. 684–690.
- [8] Y. Wang and N. Wang, "Moving-target travelling salesman problem for a helicopter patrolling suspicious boats in antipiracy escort operations," *Expert Systems with Applications*, vol. 213, p. 118986, 2023.
- [9] R. S. de Moraes and E. P. de Freitas, "Experimental analysis of heuristic solutions for the moving target traveling salesman problem applied to a moving targets monitoring system," *Expert Systems with Applications*, vol. 136, pp. 392–409, 2019.
- [10] A. Stieber and A. Fügenschuh, "Dealing with time in the multiple traveling salespersons problem with moving targets," *Central European Journal of Operations Research*, vol. 30, no. 3, pp. 991–1017, 2022.
- [11] C. D. Smith, *Assessment of genetic algorithm based assignment strategies for unmanned systems using the multiple traveling salesman problem with moving targets*. University of Missouri-Kansas City, 2021.
- [12] C. S. Helvig, G. Robins, and A. Zelikovsky, "The moving-target traveling salesman problem," *Journal of Algorithms*, vol. 49, no. 1, pp. 153–174, 2003.
- [13] M. Hammar and B. J. Nilsson, "Approximation results for kinetic variants of tsp," in *Automata, Languages and Programming: 26th International Colloquium, ICALP'99 Prague, Czech Republic, July 11–15, 1999 Proceedings 26*. Springer, 1999, pp. 392–401.
- [14] M. W. Savelsbergh, "Local search in routing problems with time windows," *Annals of Operations research*, vol. 4, pp. 285–305, 1985.
- [15] Y. Ding, B. Xin, L. Dou, J. Chen, and B. M. Chen, "A memetic algorithm for curvature-constrained path planning of messenger uav in air-ground coordination," *IEEE Transactions on Automation Science and Engineering*, vol. 19, no. 4, pp. 3735–3749, 2022.

[16] S. L. Smith and F. Imeson, "Glns: An effective large neighborhood search heuristic for the generalized traveling salesman problem," *Computers & Operations Research*, vol. 87, pp. 1–19, 2017.

[17] S. Röpke, "Palns-a software framework for parallel large neighborhood search," in *Metaheuristic International Conference*, 2009.

[18] Y. Dumas, J. Desrosiers, E. Gelinas, and M. M. Solomon, "An optimal algorithm for the traveling salesman problem with time windows," *Operations research*, vol. 43, no. 2, pp. 367–371, 1995.

[19] A. G. Philip, Z. Ren, S. Rathinam, and H. Choset, "A mixed-integer conic program for the moving-target traveling salesman problem based on a graph of convex sets," *arXiv preprint arXiv:2403.04917*, 2024.

[20] A. Stieber, "The multiple traveling salesperson problem with moving targets," Ph.D. dissertation, BTU Cottbus-Senftenberg, 2022.

[21] A. G. Philip, Z. Ren, S. Rathinam, and H. Choset, "A mixed-integer conic program for the multi-agent moving-target traveling salesman problem," *arXiv preprint arXiv:2501.06130*, 2025.

[22] ———, "C*: A new bounding approach for the moving-target traveling salesman problem," *IEEE Transactions on Robotics*, vol. 41, pp. 4663–4678, 2025.

[23] J.-M. Bourjolly, O. Gurtuna, and A. Lyngvi, "On-orbit servicing: a time-dependent, moving-target traveling salesman problem," *International Transactions in Operational Research*, vol. 13, no. 5, pp. 461–481, 2006.

[24] B. Li, B. R. Page, J. Hoffman, B. Moridian, and N. Mahmoudian, "Rendezvous planning for multiple auvs with mobile charging stations in dynamic currents," *IEEE Robotics and Automation Letters*, vol. 4, no. 2, pp. 1653–1660, 2019.

[25] N. Mathew, S. L. Smith, and S. L. Waslander, "Multirobot rendezvous planning for recharging in persistent tasks," *IEEE Transactions on Robotics*, vol. 31, no. 1, pp. 128–142, 2015.

[26] N. S. Choubey, "Moving target travelling salesman problem using genetic algorithm," *International Journal of Computer Applications*, vol. 70, no. 2, 2013.

[27] Z. Zhang, C. Chen, L. Wang, Y. Ding, and F. Deng, "A two-phase planner for messenger routing problem in uav-ugv coordination systems," *IEEE Transactions on Automation Science and Engineering*, vol. 22, pp. 16948–16963, 2025.

[28] D. J. Gulczynski, J. W. Heath, and C. C. Price, "The close enough traveling salesman problem: A discussion of several heuristics," *Perspectives in Operations Research: Papers in Honor of Saul Gass' 80th Birthday*, pp. 271–283, 2006.

[29] W. P. Coutinho, R. Q. d. Nascimento, A. A. Pessoa, and A. Subramanian, "A branch-and-bound algorithm for the close-enough traveling salesman problem," *INFORMS Journal on Computing*, vol. 28, no. 4, pp. 752–765, 2016.

[30] W. Zhang, J. J. Sauppe, and S. H. Jacobson, "Results for the close-enough traveling salesman problem with a branch-and-bound algorithm," *Computational Optimization and Applications*, vol. 85, no. 2, pp. 369–407, 2023.

[31] F. Carrabs, C. Cerrone, R. Cerulli, and C. D'Ambrosio, "Improved upper and lower bounds for the close enough traveling salesman problem," in *Green, Pervasive, and Cloud Computing: 12th International Conference, GPC 2017, Cetara, Italy, May 11–14, 2017, Proceedings 12*. Springer, 2017, pp. 165–177.

[32] F. Carrabs, C. Cerrone, R. Cerulli, and B. Golden, "An adaptive heuristic approach to compute upper and lower bounds for the close-enough traveling salesman problem," *INFORMS Journal on Computing*, vol. 32, no. 4, pp. 1030–1048, 2020.

[33] X. Wang, B. Golden, and E. Wasil, "A steiner zone variable neighborhood search heuristic for the close-enough traveling salesman problem," *Computers & Operations Research*, vol. 101, pp. 200–219, 2019.

[34] A. Di Placido, C. Archetti, and C. Cerrone, "A genetic algorithm for the close-enough traveling salesman problem with application to solar panels diagnostic reconnaissance," *Computers & Operations Research*, vol. 145, p. 105831, 2022.

[35] K. Savla, E. Frazzoli, and F. Bullo, "On the point-to-point and traveling salesperson problems for dubins' vehicle," in *Proceedings of the 2005, American Control Conference, 2005*. IEEE, 2005, pp. 786–791.

[36] L. E. Dubins, "On curves of minimal length with a constraint on average curvature, and with prescribed initial and terminal positions and tangents," *American Journal of mathematics*, vol. 79, no. 3, pp. 497–516, 1957.

[37] S. G. Manyam and S. Rathinam, "On tightly bounding the dubins traveling salesman's optimum," *Journal of Dynamic Systems, Measurement, and Control*, vol. 140, no. 7, p. 071013, 2018.

[38] J. Ny, E. Feron, and E. Frazzoli, "On the dubins traveling salesman problem," *IEEE Transactions on Automatic Control*, vol. 57, no. 1, pp. 265–270, 2011.

[39] I. Cohen, C. Epstein, and T. Shima, "On the discretized dubins traveling salesman problem," *IEEE Transactions*, vol. 49, no. 2, pp. 238–254, 2017.

[40] P. Oberlin, S. Rathinam, and S. Darbha, "Today's traveling salesman problem," *IEEE robotics & automation magazine*, vol. 17, no. 4, pp. 70–77, 2010.

[41] J. Faigl, P. Váňa, and J. Drchal, "Fast sequence rejection for multi-goal planning with dubins vehicle," in *2020 IEEE/RSJ International Conference on Intelligent Robots and Systems (IROS)*. IEEE, 2020, pp. 6773–6780.

[42] X. Ma and D. A. Castanon, "Receding horizon planning for dubins traveling salesman problems," in *Proceedings of the 45th IEEE Conference on Decision and Control*. IEEE, 2006, pp. 5453–5458.

[43] J. Drchal, J. Faigl, and P. Váňa, "Wism: Windowing surrogate model for evaluation of curvature-constrained tours with dubins vehicle," *IEEE Transactions on Cybernetics*, vol. 52, no. 2, pp. 1302–1311, 2020.

[44] K. Kučerová, P. Váňa, and J. Faigl, "Variable-speed traveling salesman problem for vehicles with curvature constrained trajectories," in *2021 IEEE/RSJ International Conference on Intelligent Robots and Systems (IROS)*. IEEE, 2021, pp. 4714–4719.

[45] S. Alatartsev, S. Stellmacher, and F. Ortmeier, "Robotic task sequencing problem: A survey," *Journal of intelligent & robotic systems*, vol. 80, pp. 279–298, 2015.

[46] L. L. Abdel-Malek and Z. Li, "The application of inverse kinematics in the optimum sequencing of robot tasks," *The International Journal Of Production Research*, vol. 28, no. 1, pp. 75–90, 1990.

[47] S. Dubowsky and T. Blubaugh, "Planning time-optimal robotic manipulator motions and work places for point-to-point tasks," *IEEE Transactions on Robotics and Automation*, vol. 5, no. 3, pp. 377–381, 1989.

[48] C. Wurll, D. Henrich, and H. Wörn, "Multi-goal path planning for industrial robots," in *1999 IEEE International Conference on Robotics and Automation (ICRA)*, 1999.

[49] M. Saha, T. Roughgarden, J.-C. Latombe, and G. Sánchez-Ante, "Planning tours of robotic arms among partitioned goals," *The International Journal of Robotics Research*, vol. 25, no. 3, pp. 207–223, 2006.

[50] F. Suárez-Ruiz, T. S. Lembono, and Q.-C. Pham, "Robotsp – a fast solution to the robotic task sequencing problem," in *2018 IEEE International Conference on Robotics and Automation (ICRA)*, 2018, pp. 1611–1616.

[51] P. T. Zacharia, E. K. Xidias, and N. A. Aspragathos, "Task scheduling and motion planning for an industrial manipulator," *Robotics and computer-integrated manufacturing*, vol. 29, no. 6, pp. 449–462, 2013.

[52] M. Verhoeven, E. H. Aarts, and P. Swinkels, "A parallel 2-opt algorithm for the traveling salesman problem," *Future Generation Computer Systems*, vol. 11, no. 2, pp. 175–182, 1995.

[53] M. Manfrin, M. Birattari, T. Stützle, and M. Dorigo, "Parallel ant colony optimization for the traveling salesman problem," in *Ant Colony Optimization and Swarm Intelligence: 5th International Workshop, ANTS 2006, Brussels, Belgium, September 4–7, 2006. Proceedings 5*. Springer, 2006, pp. 224–234.

[54] J. Schneider, C. Froschhammer, I. Morgenstern, T. Husslein, and J. M. Singer, "Searching for backbones—an efficient parallel algorithm for the traveling salesman problem," *Computer Physics Communications*, vol. 96, no. 2–3, pp. 173–188, 1996.

[55] V. V. Romanuke, "Deep clustering of the traveling salesman problem to parallelize its solution," *Computers & Operations Research*, vol. 165, p. 106548, 2024.

[56] C.-N. Fiechter, "A parallel tabu search algorithm for large traveling salesmen problems," *Discrete Applied Mathematics*, vol. 51, no. 3, pp. 243–267, 1994.

[57] Gurobi Optimization, LLC, "Gurobi Optimizer Reference Manual," 2023. [Online]. Available: <https://www.gurobi.com>

[58] J. P. Wilson, S. Gupta, and T. A. Wettergren, "Generalized multi-speed dubins motion model," *IEEE Transactions on Robotics*, 2025.

[59] Z. Chen, K. Wang, and H. Shi, "Elongation of curvature-bounded path," *Automatica*, vol. 151, p. 110936, 2023.

[60] C. Faria, F. Ferreira, W. Erlhagen, S. Monteiro, and E. Bicho, "Position-based kinematics for 7-dof serial manipulators with global configuration control, joint limit and singularity avoidance," *Mechanism and Machine Theory*, vol. 121, pp. 317–334, 2018.

[61] Y. He and S. Liu, "Analytical inverse kinematics for franka emika panda—a geometrical solver for 7-dof manipulators with unconventional design," in *2021 9th International Conference on Control, Mechatronics and Automation (ICCMA)*. IEEE, 2021, pp. 194–199.

[62] G. K. Singh and J. Claassens, "An analytical solution for the inverse kinematics of a redundant 7dof manipulator with link offsets," in *2010 IEEE/RSJ International Conference on Intelligent Robots and Systems*. IEEE, 2010, pp. 2976–2982.

- [63] J. M. Lee and J. M. Lee, *Smooth manifolds*. Springer, 2012.
- [64] R. Vershynin, “Lecture notes in geometric functional analysis,” 2009.
- [65] G. Grimmett and D. Stirzaker, *Probability and random processes*. Oxford university press, 2020.
- [66] M. Gendreau, J.-Y. Potvin *et al.*, *Handbook of metaheuristics*. Springer, 2010, vol. 2.
- [67] A. Bhat, G. Gutow, B. Vundurthy, Z. Ren, S. Rathinam, and H. Choset, “A complete algorithm for a moving target traveling salesman problem with obstacles,” in *International Workshop on the Algorithmic Foundations of Robotics*. Springer, 2024.
- [68] G. Laporte, H. Mercure, and Y. Nobert, “Generalized travelling salesman problem through n sets of nodes: the asymmetrical case,” *Discrete Applied Mathematics*, vol. 18, no. 2, pp. 185–197, 1987.
- [69] A. Bhat, G. Gutow, B. Vundurthy, Z. Ren, S. Rathinam, and H. Choset, “A complete and bounded-suboptimal algorithm for a moving target traveling salesman problem with obstacles in 3d*,” in *2025 IEEE International Conference on Robotics and Automation (ICRA)*, 2025, pp. 6132–6138.
- [70] A. Mandalika, S. Choudhury, O. Salzman, and S. Srinivasa, “Generalized lazy search for robot motion planning: Interleaving search and edge evaluation via event-based toggles,” in *Proceedings of the International Conference on Automated Planning and Scheduling*, vol. 29, 2019, pp. 745–753.
- [71] Y. Shaoul, I. Mishani, M. Likhachev, and J. Li, “Accelerating search-based planning for multi-robot manipulation by leveraging online-generated experiences,” in *Proceedings of the International Conference on Automated Planning and Scheduling*, vol. 34, 2024, pp. 523–531.
- [72] C. De Boor and C. De Boor, *A practical guide to splines*. Springer New York, 1978, vol. 27.

APPENDIX A MODIFICATION OF MEMETIC ALGORITHM

In this section, we review the memetic algorithm from [15] for the Dubins close-enough MT-TSP. We then explain how we extend [15] to deal with time windows, parallelize [15], and specialize [15] to the close-enough MT-TSP and the variable-speed Dubins MT-TSP, so that we can use it as a baseline.

A. Review of Unmodified Memetic Algorithm

[15] encodes a solution as a sequence $G = (g_1, g_2, \dots, g_{n_{\text{tar}}})$, where $g_k = (i_k, \theta_k, \Delta t_k)$. $i_k \in \mathcal{I}$ is a target index. $\theta_k \in [0, 2\pi]$ is an angle parameterizing a position along target i_k ’s disc boundary, and Δt_k is the agent’s travel duration from target i_{k-1} to target i_k (or for $k=1$, the travel duration from $q_{a,0}$ to i_1). Together, θ_k and Δt_k indicate that the agent should intercept target k at time $t_k = \sum_{l=1}^k \Delta t_l$ and

position $p_k = \tau_{i_k}(t_k) + r_{i_k} \begin{bmatrix} \cos \theta_k \\ \sin \theta_k \end{bmatrix}$. While [15] considers

a Dubins car, the solution encoding does not specify the agent’s heading angle at each target and thus could map to several different agent trajectories. To decode a sequence $G = (g_1, g_2, \dots, g_{n_{\text{tar}}})$ into a single agent trajectory, [15] begins with a trajectory of zero duration starting at $q_{a,0}$ and time 0. [15] then iterates from $k=1$ to n_{tar} , where at each iteration, [15] appends a new trajectory segment to its existing trajectory, terminating at some configuration $q_{a,k}$. To generate this trajectory segment and $q_{a,k}$, [15] computes a path from $q_{a,k-1}$ to p_k , with relaxed terminal heading, with maximum curvature $\frac{1}{\rho}$ and length $v\Delta t_k$, where v and ρ are the fixed speed and fixed minimum turning radius considered by [15]. The trajectory segment for iteration k is obtained by moving

the agent along the computed path with speed v . Letting the terminal heading of the path be $\phi_{a,k}$, we have $q_{a,k} = (p_k, \phi_{a,k})$.

[15] begins by initializing a population of n_{pop} solutions, $P = \{G_1, G_2, \dots, G_{n_{\text{pop}}}\}$, then at each iteration, generates a new population by applying the following operations to each solution G_m in the current population, in order: crossover, mutation, repair, and transformation. Crossover randomly selects another solution G_n at random from P , then constructs a solution ${}^{\text{cros}}G_m$ using portions of G_m and G_n . Mutation randomly perturbs ${}^{\text{cros}}G_m$ to generate a solution ${}^{\text{mut}}G_m$. Since crossover and mutation may produce an infeasible solution (i.e. where no curvature-bounded path with length $v\Delta t_k$ exists from $q_{a,k}$ to p_k in the decoding procedure above), repair is applied to ${}^{\text{mut}}G_m$ to generate a feasible solution ${}^{\text{rep}}G_m$.

To repair a solution ${}^{\text{mut}}G_m = (g_1, g_2, \dots, g_{n_{\text{tar}}})$, [15] iterates from $k=1$ to n_{tar} , where each iteration k finds a Δt_k such that a curvature-bounded path with length $v\Delta t_k$ exists from $q_{a,k-1}$ to p_k . We refer to a Δt_k satisfying these conditions as *kinematically feasible*. [15] finds a kinematically feasible Δt_k by applying Newton’s method to the root-finding problem $v\Delta t_k - d(\Delta t_k) = 0$, where $d(\Delta t_k)$ is the length of the shortest Dubins path with free terminal heading from $q_{a,k-1}$ to $\tau_{i_k}(t_{k-1} + \Delta t_k)$. [15] terminates Newton’s method when it finds a kinematically feasible Δt_k , which is not necessarily a root for the root-finding problem.

After generating a solution ${}^{\text{rep}}G_m$ via repair, [15] performs a transformation step, which aims to modify the Δt_k values in ${}^{\text{rep}}G_m$ to produce a lower-cost solution ${}^{\text{trans}}G_m$. The transformation iterates from $k=1$ to n_{tar} and attempts to minimize Δt_k while keeping other values in the encoding fixed. The minimization is formulated as the same root-finding problem as the repair step, but now [15] iterates until $|v\Delta t_k - d(\Delta t_k)| < 0.01$. After generating ${}^{\text{trans}}G_m$, for each G_m , [15] selects a random subset of the top 50% of solutions, then applies additional local search methods to improve the θ_k values of the selected solutions.

B. Modification to Handle Time Windows

The first part of [15] that we modify to handle time windows is the initial population construction. To construct an initial population, [15] generates n_{pop} solutions by randomly sampling different sequences of g_k values. We found that in the presence of time windows, this method often generated infeasible solutions, so we instead generate the initial population by running Alg. 2 n_{pop} times with different random seeds.

We additionally modify the repair step to handle time windows. In particular, when using Newton’s method for root-finding at iteration k , we clip Δt_k iterates to the range $[\underline{t}_{i_k} - t_{k-1}, \bar{t}_{i_k} - t_{k-1}]$. It may be the case that there is no kinematically feasible $\Delta t_k \in [\underline{t}_{i_k} - t_{k-1}, \bar{t}_{i_k} - t_{k-1}]$. To handle this complication, before running Newton’s method, we check if $t_{k-1} > \bar{t}_{i_k}$, and if so, we terminate the repair step. We discuss additional early termination conditions for the repair step that are specific to the close-enough MT-TSP and variable-speed Dubins MT-TSP in Appendix A-D and A-E. If we terminate the repair without obtaining a kinematically feasible $\Delta t_k \in [\underline{t}_{i_k} - t_{k-1}, \bar{t}_{i_k} - t_{k-1}]$, we skip

the transformation step and set ${}^{\text{trans}}G_m$ equal to G_m . We also modify the transformation step to handle time windows in ways specific to each problem variant, discussed in Appendix A-D and A-E.

C. Parallelization

We parallelize the initial population construction of [15] by parallelizing Alg. 2, using the methods described in Section VII. We also perform crossover, mutation, repair, and transformation on different solutions G_k in different threads. Finally, we parallelize the local search as follows. In one of its local search methods, [15] chooses some $k \in \mathcal{I}$ at random, samples different candidate values $\tilde{\theta}_k^1, \tilde{\theta}_k^2, \dots, \tilde{\theta}_k^{n_{\text{sample}}} \in [0, 2\pi]$, then sets θ_k to the sample giving the largest cost improvement. We evaluate the cost improvement for all the samples in parallel.

D. Specialization to Close-Enough MT-TSP

Our specialization of [15] to the close-enough MT-TSP relies on the fact that in all instances we generated, targets' speeds are no larger than the agent's maximum speed. We checked this condition for each instance as follows. First, using the fact that the targets' trajectories are B-splines, we computed the velocity B-spline for each target. Next, we computed the norm of each control point, and we let \bar{v}_i be the maximum of these norms for target i . Let \mathcal{D}_i be the disc of radius \bar{v}_i centered at the origin of \mathbb{R}^2 . All the velocity B-spline control points for target i are contained in \mathcal{D}_i . Combining this fact with the convexity of \mathcal{D}_i , we know that the convex hull of the control points is contained in \mathcal{D}_i . A B-spline is contained in the convex hull of its control points [72], which means that target i 's velocity always lies in \mathcal{D}_i and thus has norm no larger than \bar{v}_i . We verified that for all targets, $\bar{v}_i \leq v_{\max}$, which verifies that targets in our instances move with speed no faster than v_{\max} .

Before running Newton's method during iteration k of the repair step, we check if the agent can feasibly meet target i_k at the end of its time window, i.e. we check if $\|\tau_{i_k}(\bar{t}_{i_k}) - q_{a,k-1}\| \leq v_{\max}(\bar{t}_{i_k} - t_{k-1})$. If not, $\bar{v}_{i_k} \leq v_{\max}$ implies that the agent cannot meet target i_k within its time window (see [22], Theorem 2), and we terminate the repair step. On the other hand, if $\|\tau_{i_k}(\bar{t}_{i_k}) - q_{a,k-1}\| \leq v_{\max}(\bar{t}_{i_k} - t_{k-1})$, we run Newton's method, starting at the value of Δt_k from ${}^{\text{mut}}G_m$, until we find a kinematically feasible $\Delta t_k \in [\bar{t}_{i_k} - t_{k-1}, \bar{t}_{i_k} - t_{k-1}]$.

Finally, we modified the transformation procedure for the close-enough MT-TSP. The transformation from [15] attempts to minimize Δt_k , which only minimizes distance traveled for a fixed-speed agent. To handle a variable-speed agent, we use projected gradient descent to find Δt_k that minimizes the straight-line distance from $q_{a,k-1}$ to $\tau_{i_k}(t_{k-1} + \Delta t_k)$.

E. Specialization to Variable-Speed Dubins MT-TSP

To specialize [15] to the variable-speed Dubins MT-TSP, we remove the θ_k values from the solution encoding, and thus we remove the local search on the θ_k values as well. Additionally, during iteration k of the repair step, we perform the root-finding described in Appendix A-A for each $v \in \mathcal{S}_{\text{speed}}$, rather

than for a single speed. We run Newton's method until either (i) $|v\Delta t_k - d(\Delta t_k)| < 0.01$, (ii) two consecutive Δt_k iterates are the same, or (iii) we reach a maximum number of iterations n_{rep} . To determine n_{rep} , we ran our modification of [15] on 10 instances with 50 targets, initially with $n_{\text{rep}} = 1000$. Newton's method never needed more than 276 iterations to succeed, so we rounded to the nearest hundred and set $n_{\text{rep}} = 300$.

After performing a Newton solve for each v at iteration k of a repair, we have up to one Δt_k for each v . If we have a Δt_k for any of the v 's, we choose the smallest Δt_k . This procedure attempts to minimize Δt_k , rather than the original method from [15], which simply seeks a kinematically feasible Δt_k . While we initially attempted methods that stopped the k th repair iteration as soon as they found a kinematically feasible Δt_k , this resulted in fewer repairs succeeding and larger solution costs. This is in contrast to the close-enough MT-TSP, where we found that minimizing Δt_k up to a tolerance resulted in higher solution cost (distance traveled) than if we stopped at a kinematically feasible Δt_k .

We additionally modified the transformation step as follows. During iteration k of the transformation, while [15] attempts to minimize Δt_k for a fixed speed, we perform the minimization for each $v \in \mathcal{S}_{\text{speed}}$. We then choose the v resulting in the minimum $v\Delta t_k$, aiming to minimize distance traveled. We use Newton's method to solve the underlying root-finding problem and perform the same clipping and termination conditions as in the repair step to handle time windows.